3-27-2020

Detection of Human Vigilance State During Locomotion Using Wearable FNIRS

MASUDUR R. SIDDIQUEE
Florida International University, msidd021@fiu.edu

FLORIDA INTERNATIONAL UNIVERSITY

Miami, Florida

DETECTION OF HUMAN VIGILANCE STATE DURING LOCOMOTION USING WEARABLE FNIRS

A dissertation submitted in partial fulfillment of

the requirements for the degree of

DOCTOR OF PHILOSOPHY

in

ELECTRICAL AND COMPUTER ENGINEERING

by

Masudur R. Siddiquee

2020

To: Dean John L. Volakis
College of Engineering and Computing

This dissertation, written by Masudur R. Siddiquee, and entitled Detection of Human Vigilance State During Locomotion Using Wearable fNIRS, having been approved in respect to style and intellectual content, is referred to you for judgment.

We have read this dissertation and recommend that it be approved.

_____
Armando Barreto

_____
Gang Quan

_____
Jean H. Andrian

_____
Wei-Chiang Lin

_____
Ou Bai, Major Professor

Date of Defense: March 27, 2020

The dissertation of Masudur R. Siddiquee is approved.

_____
Dean John L. Volakis
College of Engineering and Computing

_____
Andrés G. Gil
Vice President for Research and Economic Development
and Dean of the University Graduate School

Florida International University, 2020

DEDICATION

To my dearest Naznin and my parents

ACKNOWLEDGMENTS

First, I would like to express gratitude to my advisor Dr. Ou Bai for his patience, motivation and immense knowledge. His mentorship helped me grow both personally and professionally. He never hesitated to devote his time, regardless of day or night, to discuss the research.

I want to thank the members of the committee, Dr. Quan, Dr. Barreto, Dr. Andrian, and Dr. Lin, for taking the time to evaluate and comment on this dissertation.

A special thanks to my friends and colleagues in the Human Cyber Physical Systems (HCPS) lab, Roozbeh, Sebastian, Tushar, Rod, Tong, Robin, and Connie for their support and help throughout various stages of the research.

My deepest gratitude to my parents and siblings, without their support, this would not have been possible. A special thanks to Farzana and Labiba for being there when I was going facing the tough times and found a way to help me navigate through it. I would like to thank Jalal, Shagufta, Tani, Nafis, Amit, Akash, Proyash and many others for their cordial support during this journey.

This research was supported by the Graduate assistantship from the Department of Electrical and Computer Engineering at Florida International University and National Science Foundation (CNS-1552163).

ABSTRACT OF THE DISSERTATION

DETECTION OF HUMAN VIGILANCE STATE DURING LOCOMOTION USING WEARABLE FNIRS

by

Masudur R. Siddiquee

Florida International University, 2020

Miami, Florida

Professor Ou Bai, Major Professor

Human vigilance is a cognitive function that requires sustained attention toward change in the environment. Human vigilance detection is a widely investigated topic which can be accomplished by various approaches. Most studies have focused on stationary vigilance detection due to the high effect of interference such as motion artifacts which are prominent in common movements such as walking. Functional Near-Infrared Spectroscopy is a preferred modality in vigilance detection due to the safe nature, the low cost and ease of implementation. fNIRS is not immune to motion artifact interference, and therefore human vigilance detection performance would be severely degraded when studied during locomotion. Properly treating and removing walking-induced motion artifacts from the contaminated signals is crucial to ensure accurate vigilance detection. This study compared the vigilance level detection during both stationary and walking states and confirmed that the performance of vigilance level detection during walking is significantly deteriorated (with a $p<0.05$). Further, this study explored motion artifact removal and applied machine learning methods. Results reveal

the vigilance detection during walking has a comparable performance to the stationary state when the motion artifacts are estimated and removed.

TABLE OF CONTENTS

LIST OF TABLES

LIST OF FIGURES

LIST OF ACRONYMS AND ABBREVIATIONS

NASA-TLX	National Aeronautics and Space Administration Task Load Index
BOLD	Blood Oxygen Level-Dependent Signal
EEG	Electroencephalography
fMRI	Functional Magnetic Resonance Imaging
TCDS	Transcranial Doppler Sonography
fNIRS	functional Near-Infrared Spectroscopy
IED	Improvised Explosive Devices
PET	Positron Emission Tomography
MEMS	Microelectromechanical systems
IMU	Inertia Measurement Unit
SNR	Signal to Noise Ratio
AR	Autoregressive Modelling
ARX	Autoregressive Model with Exogenous Input
ANC	Adaptive Noise Cancellation
LS	Least-Squares
NIR	Near Infra-Red
LED	Light-Emitting Diode
PD	Photodetectors
ADC	Analog to Digital Converter
CMMR	Common-Mode Rejection Ratio
MISO	Multiple Input Single Output
HbO2	Oxygenated Hemoglobin

Hb	Deoxygenated Hemoglobin
BCI	Brain Computer Interface
PFC	Pre-Frontal Cortex
ROI	Region of Interest
DA	Discriminant Analysis
SVM	Support Vector Machine
ANN	Artificial Neural Network
SFS	Sequential Forward Selection
HF	Hippocampal Formation
IPL	Inferior Parietal Lobule
PEBL	Psychology Experiment Building Language
MBLL	Modified Beer-Lambert Law
LDA	Linear Discriminant Analysis
KNN	k-Nearest Neighbors
GBT	Gradient Boosting Classifier

CHAPTER 1 INTRODUCTION

1.1 Vigilance

The human brain is a complicated and vital part of the human body. It is involved in various crucial functions, such as interpreting the sensory feedback from stimuli, staying vigilant and so on. Vigilance is the ability to maintain sustained attentional [1] focus toward external events, perceivable by any sensory input such as visual or auditory, over a prolonged period. This attentional focus, in turn, increases the neural activity [2] due to the increased cognitive workload. The energy needed for this increased cognitive workload increases the oxygen consumption in the cerebral cortex, which is later regulated by the brain's control mechanism called glial regulation [3]. Conventionally, this cognitive workload increase is measured using a subjective test such as NASA-TLX [4]. However, the above blood oxygen dependent phenomenon arises from the vigilance or cognitive workload level change, makes it possible to measure it objectively using physiological signals [5]–[8].

1.2 Detectable Brain signals related to vigilance

There are two basic types of detectable signals related to the neural activity of the brain. The electrical activity due to the synchronous firing of neurons and blood oxygen level-dependent signal (BOLD) due to the change in the oxygenation change of the brain tissue. The only modality that uses the electrical activity of neurons arise from brain functions is the Electroencephalography (EEG). On the other hand, there are several modalities to detect brain signals related to BOLD that arise due to various brain functions. For instance, Functional Magnetic Resonance Imaging (fMRI) uses the magnetic property change due to BOLD [9], Transcranial Doppler Sonography (TCDS)

uses the speed change of blood flow due to BOLD [10] and functional Near-Infrared Spectroscopy (fNIRS) uses the optical property change of the blood due to BOLD [11]. Although fMRI is considered as the de facto standard in detecting cerebral regional blood oxygen concentration change [12]–[15], fNIRS is a less expensive technology with higher portability, higher temporal resolution, but with a comparable result to fMRI [13], [14], [16]–[18]. In the case of EEG application in cognitive workload assessment [19]–[21], though it is capable of high temporal and spatial resolution, it is less portable and less immune to ambient electrical noise, which is not present in fNIRS due to its optical nature of technological implementation.

1.3 Motivation

Generally, sustained attention or vigilance is assumed to be easy to maintain, although a recent study by Warm et al. proved it requires hard mental work [22]. Moreover, detecting human vigilance levels during natural locomotion and ensuring a highly active level of vigilance state sometimes becomes essential for survivability during surveillance or combat [23]. For instance, over 70 Canadian soldiers have lost their lives due to Improvised Explosive Devices (IED) in convoy operation, and soldier vigilance was accounted as a key parameter for their survivability [24]. On the other hand, vigilance detection during locomotion is required for the betterment of basic human functions, such as gait recovery training for patients with impaired locomotion due to central nervous system injury [25]. Moreover, Intelligent Tutoring Systems, such as the adaptive tutoring system used in various military task training could also benefit from the detected

vigilance state for locomotion associated vigilance training [26], [27] as feedback to the adaptive system rather than the text-based objective input in the current feedback system.

The research on the state-of-the-art technologies for brain imaging and sensing in the last few decades has led to the development of various modalities to detect brain functions, such as fMRI, Positron Emission Tomography (PET), TCDS and fNIRS. These modalities have been successfully used to monitor human vigilance level or cognitive state in static situations such as monitoring operator cognitive workload during air traffic control [28], train driving [29], car driving [30] and so on [31]. However, these modalities pose several challenges for the application of vigilance detection, specifically when discussing non-static situations. Limitations such as the physical sizing of the systems, technological complexity, wearability, and so on make these technologies less suitable to detect vigilance level during locomotion. Specifically, two major challenges, namely detection of and removal of gait associated motion artifacts and optimization of wearability of vigilance detection systems have not been addressed. The major questions requiring investigation for accurate vigilance detection during gait are listed as follows:

Question (1): How much improvement in artifacts estimation and removal can be achieved using multi-sensor motion sensing and sensor fusion method.

Question (2): How does the reduction in sensing location on the human forehead for improved wearability affect the vigilance detection accuracy?

Question (3): How do the gait associated motion artifacts affect accurate vigilance detection during gait.

CHAPTER 2 FNIRS MOVEMENT ARTIFACTS REMOVAL

2.1 Introduction

The absorption coefficient by human tissue in the near-infrared light region of 700-1000nm [32] is much lower than other wavelength lights in the spectrum that are harmless to the human body. This property leads to the development of Near-Infrared Spectroscopy (NIRS) as a widely used method for detecting oxy- and deoxyhemoglobin levels in the blood. The NIRS signal can be detected by illuminating the human body with light from the near-infrared region [11], [33]. Moreover, the non-invasiveness, safety and cost-effectiveness [34] make NIRS even more popular than any other method of detecting blood oxygenation level. The level of blood oxygenation in various parts of the human body convey a great deal of information about various physiological phenomena and processes [35], such as cardiovascular disease [36] and sepsis [37] from muscle oxygenation, cognitive involvement [16], [38] and activation of brain function [39], [40] from cerebral oxygenation.

Movement artifact removal is one of the most challenging parts of any bio-signal processing and the NIRS for blood oxygen level detection is no exception. Although electrical noise [41] is a prominent problem in any electrical system for sensing [42]–[44], it is not the case for fNIRS system. The problem in fNIRS is that it is not possible to fully restrict a subject from movement, voluntary or involuntary, and thus the acquired bio-signals are contaminated by the movement artifacts in different extents. Sometimes this contamination is so prominent that the subtle changes correspond to physiological changes subdued by the artifacts; thus, the usability of the acquired signal mostly depends on the successful removal of the movement artifacts [45]. In the NIRS, the light source

and the detectors are directly coupled to the human skin and this coupling is easily altered [46] by movement artifacts, which result in coupling error [47]. This coupling error imposes high uncertainty in the detection of the true changes in the NIRS signal which corresponds to the change in the physiological phenomena [48]. Moreover, from the perspective of the frequency domain, the NIRS signal variation due to the physiological change and the changes due to the motion artifacts are closely overlapped with each other, which makes it harder to separate the movement artifact content from the signal.

2.2 Related Works

Numerous artifacts removal techniques for NIRS have been developed in the last few decades [17], [49]–[54]. Most of them use the nature of the signal itself and the theoretical assumption of the influence of the movement artifact on the detected signal. A Majority of these methods development direction lies in the fact that detecting any other signal highly correlated to the movement artifacts was not readily available or difficult [55]. But the recent improvements in the Microelectromechanical systems (MEMS) chip components that are capable of registering motion information, i.e. acceleration, yaw, pitch, roll, etc., make it possible to observe motion-related signal concurrently with bio-signals of interest for various biomedical applications [56]–[61]. With respect to NIRS signal detection, this advancement in the MEMS chip component makes it possible to record movement artifacts related motion data and the NIRS signal simultaneously [62]–[64]. This additional information related to movement artifact leads to the more effective use of the adaptive noise cancellation technique on the NIRS signal. So far, all the research articles related to adaptive filtering to remove movement artifacts from the NIRS signal uses only the three-channel accelerometer data to estimate the movement artifacts

[57], [62], [63], [65]. In this study, nine-channel Inertia Measurement Unit (IMU) data, namely accelerometer, gyroscope, and magnetometer, are used to estimate the movement artifacts in NIRS signal and subsequently to remove the motion-related movement artifact. The basis of the study is that the more information correlated to movement artifacts available, the better the estimation of the interfering artifacts contribution on the detected signal, and greater signal to noise ratio (SNR) improvement can be achieved. Movement artifacts arise from diverse body movements, which might have very little acceleration, but a more rotational or directional change would be better registered by gyroscope and magnetometer would result in better estimation of the movement artifacts.

Movement artifacts removal techniques commonly employ the autoregressive modeling (AR) to remove the artifacts from the NIRS signal [54], [66]. In this study, the Autoregressive model with exogenous input (ARX) was used as the method to estimate the movement artifacts, and the multi-channel IMU data served as the exogenous input to the system.

Adaptive Noise Cancellation(ANC) was widely used in various fields for noise cancellation [67]. In this approach, one or more additional channels of information that is highly correlated to the interfering noise component in the primary recorded signal is used to remove the noise. The ARX modeling can be assumed as an altered method of ANC, which applies the classical least-squares (LS) algorithm to estimate the noise using exogenous input as the reference source for indirect noise estimation in the observed signal. ARX modeling is extensively used in the problems related to system identifications. In the current study, IMU signals were used as the inputs to the ARX

modeling to estimate the movement artifacts in the NIRS signal and then subtracted to estimate the true NIRS signal.

2.3 Materials and Methods

2.3.1 Data acquisition method:

In this study, data acquisition with a single wavelength and a dual-wavelength NIR light source were used during the recording from the subjects. The methodology presented in [49] was used to quantitatively assess improvement in the signal quality after the removal of the artifacts. The methodology requires that two versions of the same NIRS channels are positioned as close as possible where one is impacted by movement artifacts and another remains unimpacted. In this respect, the unaffected signal is analogous to the "ground truth" signal presented in [49], which was denote here as "reference ground truth" as the actual “ground truth” cannot be acquired. For the first two subjects, the single-wavelength LED was used with simulated artifacts, and signal quality improvement with respect to SNR and correlation was used for quantitative assessment. For the remaining two other subjects, a dual-wavelength NIR light source was used to record the data with the actual movement of the subjects causing the movement artifacts. As the NIRS signal from the last two subjects were recorded using two wavelengths, the NIRS signals can be converted to blood oxygenation concentration changes using the Modified Beer-Lambert law [68], [69] and the result of artifact removal can be compared to the expected hemodynamic changes. Considering that the hemodynamic change is minimal during a short duration when movement occurs, the levels of oxygenated (HbO_2) and deoxygenated (Hb) hemoglobin concentration will be stable before and after movement occurs. Based on this, after the movement artifact removal from the

contaminated portion of the NIRS signal, a minimal hemodynamic change with stable HbO_2 and Hb levels is expected.

2.3.2 Sensor System

To accomplish the above mentioned NIRS signal acquisition along with the simultaneous recording of multi-channel IMU data, a custom-made wearable NIRS system, based on Texas Instrument (TI) CC3200 chip, was developed incorporating other peripheral chips and using the sensor node architecture developed in [70] depicted by Figure 1. The IMU chip used in this architecture is MPU9250 which has a 3-axis accelerometer, 3-axis gyroscope and 3-axis magnetometer data acquisition capability with a 16-bit resolution for each channel, and the chip was attached to the NIR detector for better registration of the movement artifacts impact at the detector. In this study, each IMU channel was sampled at 62.5 Hz. An 850nm wavelength LED and another 850nm and 770nm dual-wavelength LED are used as the source of NIR light, and as the detector, a photodiode chip from TI modeled as OPT101 was used, which incorporate the required trans-impedance amplifier in the same chip. To digitize the analog signal from OPT101, a high precision analog to digital converter (ADC) chip from TI, with part no ADS1292, was used, which has a 24-bit resolution and high common-mode rejection ratio (CMMR) and support two-channel input. This ADC supports multiple sampling rates ranging from 860 Hz to 8000 Hz, and we sampled the NIRS signal at 1000 Hz. To minimize the bus contention by the two vital peripheral devices in the system, IMU and ADC, these devices were connected to the main processor unit via the different buses, I2C and SPI, respectively. The main processor unit used in this sensor architecture, CC3200, house two separate MCU in the same chip; one is featuring Wi-Fi Internet-On-a-Chip and

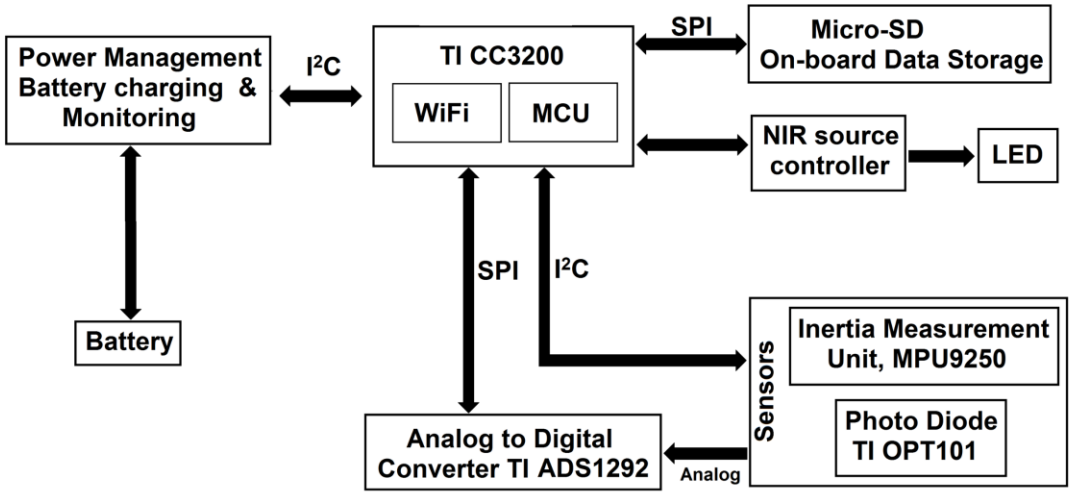

Figure 1. NIRS cyber-system Hardware Architecture

another one as a typical microcontroller. Thus, the system can simultaneously collect the data from the peripheral devices and transfer those wirelessly through the internet to a remote system or any local computer connected to the system using Wi-Fi.

2.3.3 ARX modeling and artifacts removal

The artifacts estimation and removal process are outlined in Figure 2. Let $s[n]$ denote the true hemodynamic signal, which was distorted by the motion artifacts signal $w[n]$. This corrupted hemodynamic signal $x[n]$ detected by the NIRS sensor can be expressed as,

$$x[n] = s[n] + w[n] \qquad \text{Eq. 1-1}$$

We used ARX modeling to estimate the motion artifacts in the detected signal. It is a widely used method in system identification task to determine the model structure using the input-output data. In this respect, it uses the least-squares method to estimate the best set of the coefficient of the system model from the input-output data available. In our study, the system resembled a multiple-input single-output (MISO) model, because the

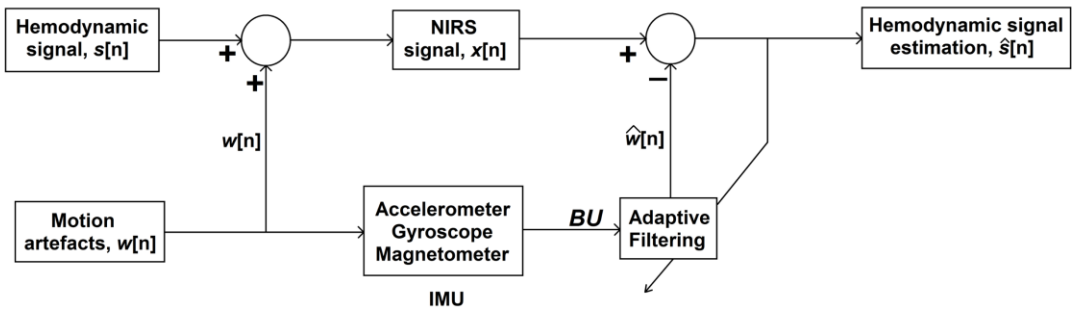

Figure 2. Block diagram of artifacts removal process.

IMU data inputted into the model consisted of multiple channel data. In this case, the ARX modeling can be represented using the following equation,

$$\hat{w}[k] = a_1 x[k-1] + a_2 x[k-2] + \cdots + a_{NA} x[k-NA] + \boldsymbol{b_0^T u}[k] + \boldsymbol{b_1^T u}[k-1] + \cdots + \boldsymbol{b_{NB}^T u}[k-NB] \quad \text{Eq. 1-2}$$

Here $x[n]$ is the detected NIRS signal and $\boldsymbol{u}[k]$ is the IMU data. Here $\hat{w}[n]$ is the output from the system based on the model coefficients $\boldsymbol{a} = [a_1\ a_2\ \cdots\ a_{NA}]$ and $\boldsymbol{B} = [\boldsymbol{b_0}\ \boldsymbol{b_1} \cdots \boldsymbol{b_{NB}}]$ when the input to the model is $\boldsymbol{U} = [\boldsymbol{u}[k]\ \boldsymbol{u}[k-1] \cdots \boldsymbol{u}[k-NB]]$. The model coefficients $\boldsymbol{a}$ and $\boldsymbol{B}$ selection in ARX modeling can be depicted by the following equation, which is also known as the least square method,

$$J(\boldsymbol{a}, \boldsymbol{B}) = \sum_{k=1}^{N} (x[k] - \hat{w}[k])^2 \quad \text{Eq. 1-3}$$

where $\boldsymbol{b_0^T}\ \boldsymbol{b_1^T} \cdots \boldsymbol{b_{NB}^T}$ are $1 \times L$ coefficient vectors and $\boldsymbol{u}[k]$ is a $L \times 1$ input vector, and the dimension L is the number of IMU data channel used. There were three combination cases for $\boldsymbol{U}$ used in this study, and they were,

Case 1: $\boldsymbol{u}[k] = \left[A_x[k]\ A_y[k]\ A_z[k]\right]^T;\ L = 3$

Case 2: $\boldsymbol{u}[k] = \left[A_x[k]\ A_y[k]\ A_z[k]\ G_x[k]\ G_y[k]\ G_z[k]\right]^T;\ L = 6$

Case 3: $\boldsymbol{u}[k] = \left[A_x[k]\ A_y[k]\ A_z[k]\ G_x[k]\ G_y[k]\ G_z[k]\ M_x[k]\ M_y[k]\ M_z[k]\right]^T ; L = 9$

For the conventional studies [54], [62], [64], [65] where only three channels Accelerometer data are used for autoregressive modeling, $\boldsymbol{U}$ can be expressed as in case 1 where A_x, A_y and A_z represent the three channels of Accelerometer data. Additional to the conventional study using only three channels of Accelerometer data, we extended the study using six channels and nine channels of IMU data. In cases 2 and 3, G_x, G_y and G_z represent the three channels of Gyroscope data and M_x, M_y and M_z represent the three channels of Magnetograph data.

In the artifact estimation process, the portion of the NIRS signal containing movement artifacts was fed to the ARX modeling algorithm as the output and the corresponding multichannel IMU data as the input to determine the model coefficients. For each artifact segment, this operation was iterated using several combinations of model orders from 1 to 10 and the order selected for who's the sum of squared error was the minimum between the estimation and the detected signal. Using the returned coefficient, a simulation model was defined for the current noisy portion of the NIRS signal. In the newly defined simulation model, the IMU signals were used as the input to the model to get the estimation $\widehat{w}[n]$. Here, the estimation closely resembled to artifact $w[n]$ as the signal contribution by the true hemodynamic signal $s[n]$ to the detected signal $x[n]$ was very small compared to the artifact's contribution. Thus, this estimated signal $\widehat{w}[n]$ was then subtracted from the observed signal $x[n]$ to get the estimation of the movement artifacts free hemodynamic signal $\hat{s}[n]$ as per the equation below,

$$\hat{s}[n] = x[n] - \widehat{w}[n] \qquad \text{Eq. 1-4}$$

2.3.4 SNR improvement:

As the data acquisition methodology used in this study was very much similar to [49], the SNR calculation was also done using a similar formula applied in that study. The difference in the SNR, before and after the removal of the artifacts, is calculated using the following equation which is described in [71],

$$\Delta SNR = 10\ log_{10}^{(\frac{\sigma_x^2}{\sigma_{e_{after}}^2})} - 10\ log_{10}^{(\frac{\sigma_x^2}{\sigma_{e_{before}}^2})} \quad \text{Eq. 1-5}$$

Where, σ_x^2 is the variance of the movement artifacts free signal which is the referenced ground truth and $\sigma_{e_{before}}^2$ and $\sigma_{e_{after}}^2$ are the variance of the signal with the movement artifacts before and after the artifacts are removed, respectively.

2.3.5 Subjects and experimental design

Four healthy subjects, ages 22, 25, 27 and 28, with no history of asphyxia or brain disorder, volunteered for this study and a total of twelve sessions of data were collected. The NIRS signals were recorded from the forehead for simplicity. All the subjects were instructed to sit comfortably during the NIRS recording. As mentioned before, the NIRS signals from the first two subjects were contaminated by simulated movement artifacts. These simulations were done by external tapping on one of the two optical sensors, while the other remained unaffected. The NIRS signals from the other two subjects were collected by dual-wavelength NIR light source, the subjects were instructed to move their head to induce natural movement artifact in the NIRS signals.

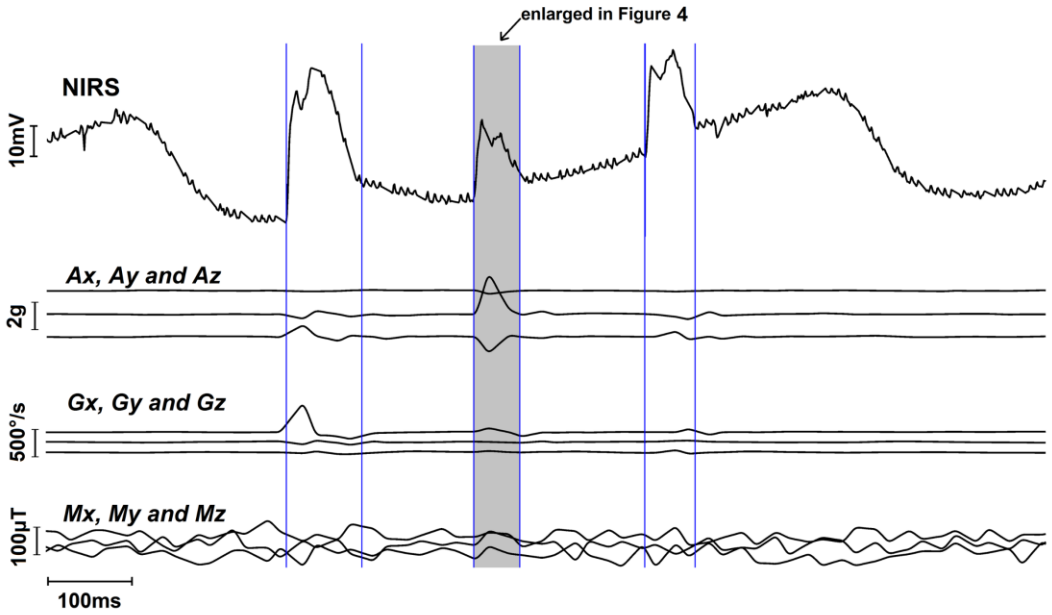

Figure 3. Raw data of one channel NIRS signal containing 3 noise segments indicated by vertical blue lines and corresponding 9 channel IMU signals

2.4 Results

In this study, the artifacts removal from the NIRS signal was implemented on the raw signal from the optical sensor. Thus, the clean signal (after the movement artifact removal) can be used in any other processing for further study. Figure 3 depicts a representative portion of the raw NIRS and the corresponding IMU data from subject 1. This NIRS signal contains three movement artifact segments which are indicated by vertical lines in the topmost plot in Figure 3. The simultaneous IMU data of this portion, which are three channels accelerometer, three channels gyroscope and three channels magnetometer data, are plotted in the same Figure 3. It is already mentioned earlier that most of the IMU-based movement artifact removal studies used three channels accelerometer data [62], [63], [65], whereas, in this study, it was observed from the raw signal that without any processing, the Gyroscope data have the most impact from the

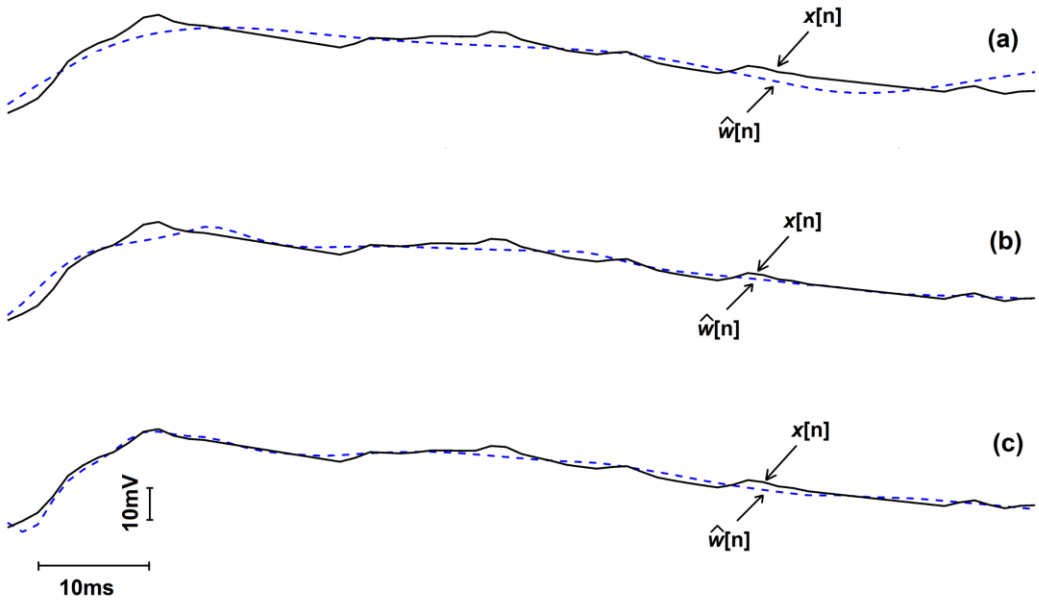

Figure 4. The estimated noise signal (blue dotted line) and the original signal (black solid line) for the second noise segment depicted in Figure 3. Plot (a) shows the result when 3 channels were used, plot (b) when 6 channels were used and plot (c) when 9 channels were used.

motion artifacts and thus highly effective in estimating the artifacts. In the signal portion presented in Figure 3, the gyroscope data have a more prominent impact on all three movement artifact segments in comparison to the accelerometer and the magnetometer data, which is apparent in Figure 3.

The movement artifact estimation for the second segment in Figure 3 is presented in Figure 4. In Figure 4, movement artifact containing signal is depicted by the solid black line, and the estimation of the movement artifact is indicated by the dashed blue line. Three estimation results are presented qualitatively in Figure 4; the plot *(a)* for the case when only accelerometer data is used to estimate, the plot *(b)* presents the estimation result when accelerometer and gyroscope data are used in the modeling and lastly bottom-most plot *(c)* shows the estimation result when all the nine-channel IMU data, namely accelerometer, gyroscope and magnetometer, were used. This qualitative

Table 1. SNR improvement of 6 representative segments of noise in the recording from the subject 1 and 2, when various number of IMU channel data were used to remove the artifacts. The correlation coefficient presented in the table is between artifacts removed signal and the ground truth signal.

Subjects	Accel.		Accel. + Gyro.		Accel. + Gyro. + Magn.	
	SNR (dB)	Correlation	SNR (dB)	Correlation	SNR (dB)	Correlation
Sub 1 Seg 1	7.92	0.79	11.33	0.82	14.77	0.83
Sub 1 Seg 2	8.93	0.89	12.66	0.92	15.11	0.93
Sub 1 Seg 3	5.31	0.94	13.92	0.96	13.92	0.96
Sub 2 Seg 1	7.35	0.96	13.44	0.97	19.08	0.97
Sub 2 Seg 2	3.04	0.77	5.29	0.78	11.95	0.98
Sub 2 Seg 3	11.56	0.94	14.31	0.95	17.46	0.95

representation indicates that the more IMU channels that were used to model, the better the estimation was, and the best estimation was achieved when all the nine channels of IMU data available were used.

The quantitative metric, to assess the performance of the artifact's removal technique used in this study was the improvement in SNR which was calculated according to the equation (1-5) described in the previous section. This same metric and calculation were also used in several other research related to artifacts removal techniques presented in [49], [54], [64], [71]. In this respect, Table 1 represents the data of SNR improvement's quantitative data for the three movement artifact segments indicated in Figure 3, which belongs to the data recorded from the subject 1 and for the data from the subject 2. For all the six segments, SNR improvements have been calculated in the cases of using three channels (only accelerometer data), six channels (accelerometer and gyroscope data) and nine channels (accelerometer, gyroscope and magnetometer). The data presented in Table 1 indicates that for all the movement artifact segments, SNR improvements are higher when gyroscope and magnetometer data are used along with the accelerometer data. Specifically, for the first movement artifact segments from subject 1, we had 11.33dB SNR when six channels were used, which was 3.41dB higher than the SNR when only

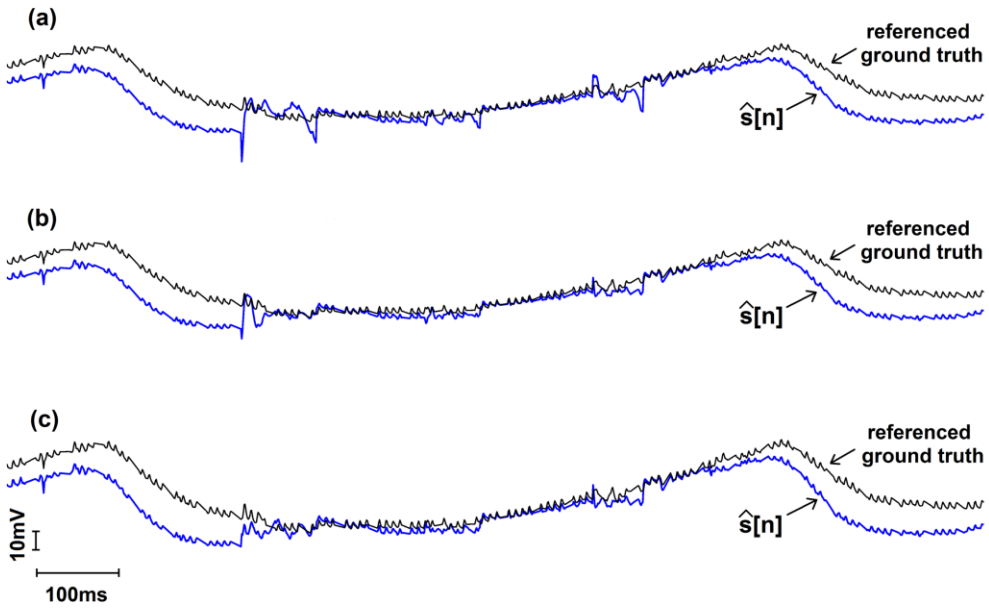

Figure 5: Qualitative representation of the NIRS signal after replacing the 3 artifacts containing segments by de-noised signal along with the referenced ground truth signal from the other NIRS channel which is analogous to "ground truth" signal. Plot (a) shows the result when three channels were used, plot (b) when six channels were used and plot (c) when nine channels were used.

three channels were used, and the SNR was 14.77dB when nine channels were used which was 6.85dB higher than the SNR we got for three channels only.

Similarly, for the second movement artifact segment, we had 15.11dB SNR which was 6.18dB higher than the SNR when we only used three channels IMU data, and for the third movement artifact segment, we had 13.92dB SNR which was 8.61dB higher than the result for the three channels only case. Additionally, we computed the correlation between the artifacts removed signal and reference ground truth signal for each movement artifact segments which are also presented in Table 1. For the first movement artifact segment, the correlation coefficient was increased from 0.79 to 0.82 when six channels IMU data were used to remove the movement artifacts than when only three channels data were used, and this value increased to 0.83 when nine channels IMU data were used. In the case of the second movement artifact segment, the correlation

coefficient was increased from 0.89 to 0.92 and 0.93 when six channels and nine channels IMU data were used respectively to remove the movement artifacts contribution in the signals. For the third movement artifact segment, the correlation between the movement artifact removed signal and the reference ground truth signal was 0.94 when only three channel IMU data were used to remove the artifacts, and it was 0.96 when six or nine-channel IMU data were used for artifacts removal.

In the data recorded from the second subject, another three movement artifact segments were selected, and all the similar processing described above were applied to those movement artifact segments. The quantitative SNR improvements for those segments are also presented in the data Table 1 which shows a similar trend in the SNR improvements for subject 1. In the case of movement artifact segments from the subject 2, we had 19.08dB SNR when we used nine channels IMU data which was 11.73dB higher than the result for three channels usage case for the first movement artifact segment. Likewise, for the second movement artifact segment from subject 2, we had 11.95dB SNR and for third segment 17.46 dB when nine channels IMU data were used which were 8.91 dB and 5.90dB higher than when six and nine channels IMU data were used, respectively. In respect of the correlation coefficient, the first movement artifact segment for this subject had a coefficient of 0.96 between movement artifact removed signal and referenced ground truth signal when three channels IMU data were used and it 0.97 when six or nine channels IMU data were used. For the second movement artifact segment, the correlation coefficient was increased from 0.77 to 0.78 and 0.99 when we increased the number of IMU channels used in artifact removal to six and nine channels, respectively, from only three channels data. The last movement artifact segment from this

subject had a correlation coefficient of 0.94 between the movement artifact removed signal and the reference ground truth when three channels IMU data were used to remove movement artifacts and 0.95 when six or nine-channel IMU data were used.

The qualitative result of removing the artifacts that contaminated the abovementioned three segments present in the recording from subject 1 is presented in the Figure 5 which are plotted with the solid blue lines, whereas the artifacts-free NIRS signals from the other channel are also concurrently plotted in the same figure using solid dark lines to indicate the empirical comparisons. Similar to the presentation used in Figure 4, the result of a various number of IMU channel data usage is presented in Figure 5, plot *(a)* represent the result when only accelerometer data were used, plot *(b)* when accelerometer along with the gyroscope data were used and finally plot *(c)* depicts the result when accelerometer, gyroscope and magnetometer data were used altogether.

In the case of quantitative results, it was easy to determine the best outcome of the artifacts removal as it was obvious from the exact values of SNR presented in the data table that the higher the SNR, the better the result is. But in the case of the empirical result, there is no direct way to determine the best. In this respect, in the current study, we assumed the artifact-free NIRS channel to be the reference ground truth signal, to compare empirically. Empirically, we can say that the closer the variance of NIRS signal after the artifacts removal to the variance of the referenced ground truth signal, the better the result is. In that sense, we can say the best result was achieved when nine channels of IMU data were used, which is also consistent with SNR improvement data presented in Table 1 and apparent from the plot *(c)* in Figure 5.

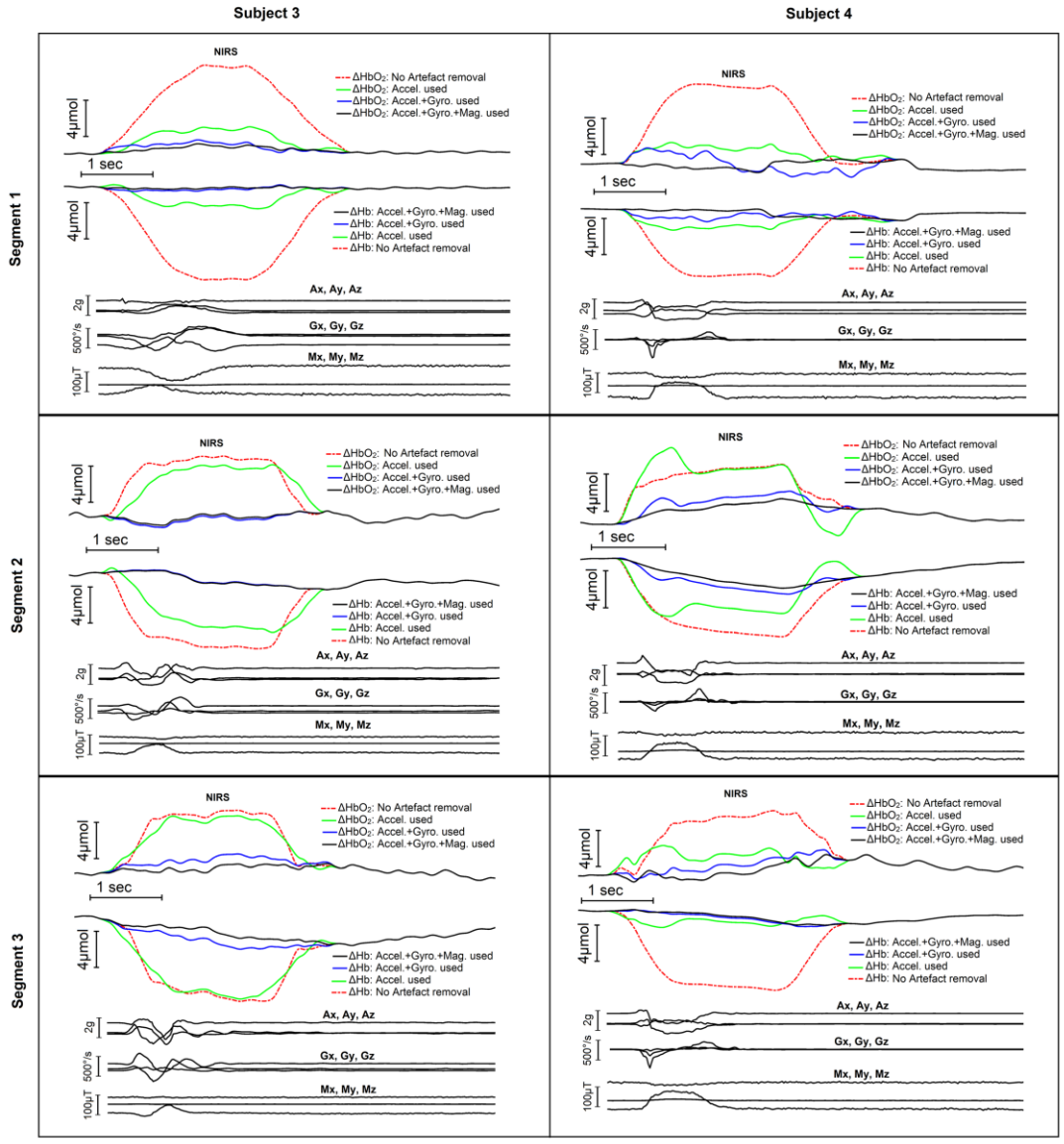

Figure 6: Effect of estimating and removing movement artifacts using multi-channel IMU signals on HbO2 and Hb change detection.

The NIRS signals from the subject 3 and 4 were recorded using dual-wavelength NIR light source so that it can be converted to oxygenated (HbO_2) and deoxygenated (Hb) hemoglobin concentration changes with typical processing. The movement artifacts were removed from the raw NIRS signal using IMU signals as described in the previous section and then converted the denoised signals to HbO_2 and Hb changes using typical

Beer-Lambert law [68]. Three noise segments data from each of the two subjects are presented in figure 6. Each of the six plots in figure 6 presents the HbO_2 and Hb change when no denoising was used, when only accelerometer signals were used, when accelerometer and gyroscope signal were used and when accelerometer, gyroscope and magnetometer signal were used for artifacts estimation and removal. In all the plots there were substantial changes in HbO_2 and Hb concentration around the movement artifacts containing parts of the signals when no denoising was used. For all the six artifact segments, HbO_2 and Hb changes curve get closer to the minimal change when artifacts estimation and removal was done for the artifacts containing part of the NIRS signal, and the case of estimating the artifacts by accelerometer, gyroscope and magnetometer result better than the case of using only accelerometer for the estimation and removal of the movement artifacts.

2.5 Discussion

In this paper, a method of using multi-channel IMU data to successfully remove movement artifacts from NIRS signal has been presented. The qualitative and quantitative results show that implementation of multi-channel IMU data resulted in more accurate modeling of motion artifacts in NIRS, and thus we obtained more accurate motion artifacts free NIRS signal, which can be used to detect physiological changes accurately.

After the first massive production of micro-electromechanical-system (MEMS) chip-based accelerometer in about 1993 [72], it was extensively used in other fields such as automobile, aerodynamics and so on; but there was a sloth progress in effectively using such devices in the field of bio-signal acquisition due to the reduction of comfort of the

subject [64] which results from the extra wiring and placement of this additional sensors. Moreover, placing the accelerometer sensor close to the NIR sensor was also another challenge as the NIRS system used in most of the research utilized the optical fiber-based light transport system [73] to and from the subject body. This close placement of the accelerometer to the light coupling to the subject body is necessary to record motion artifacts caused by the subject movement as well as due to the NIR sensor shifting [64]. These challenges were mitigated in this study by careful selection of the components used in the design of the system and making the system as wearable as possible. For instance, the IMU chip MPU9250, used in the system is only 3mm by 3mm in dimension and this IMU was attached to the body of the NIR detector sensor OPT101 chip to record the true motion of this detector as well as the movement of the subject body. The entire wireless NIRS system used in this study has a dimension of only 30mm by 48mm and power by a small lithium-ion battery, which makes it a true wearable NIRS data acquisition system. Considering the subtle details like those presented above could be helpful in designing a wearable NIRS system incorporating sophisticated chip like IMU which will improve the overall system performance.

The main challenge related to the hardware of the system in this study came from the strategy used in the acquisition of the multi-channel NIRS signals. As already mentioned earlier, to use the effective method of quantitative evaluation of the result of movement artifacts removal success, the two NIRS detectors were placed as close as possible with the target of recording a very similar version of NIRS signal where one of them are intentional movements' artifacts induced. Due to this closeness, inducing artifacts in one

NIRS channel while leaving another channel undisturbed was tough and a lot of attempts took place to achieve this data acquisition strategic goal.

The effectiveness of the regressive modeling, like the ARX used in this study to estimate motion artifacts, highly depends on how much motion-related information present in the exogenous input. The raw data presented in Figure 3 has an important finding in this context; the first and the last artifact segments have a high impact on the gyroscope data, whereas, for the middle artifact segment, the accelerometer data have a prominent impact. This finding implies that using more channels of IMU data increases the probability of capturing the motion-related data in at least some of the channels, which in turn increase the successful estimation of the movement artifacts. In this respect, the SNR improvement results presented in the Table 1 depicts that SNR improvement increased if the number of IMU data channel used in the modeling were increased except for the movement artifact segment 3 from the subject 1. For the movement artifact segment 3 from subject 1, the SNR improvement value for the six-channel and nine-channel IMU data, are the same, which is due to the fact that the last three channels of the IMU data (the magnetometer data) had an insignificant contribution on the artifact estimation. This insignificant contribution might have two reasons, either the artifact was indifferent to the variable the sensor was sensing or the sensor itself was not sensitive enough to detect the subtle change in that variable. On the other hand, for the movement artifact segment 2 from subject 2 in Table 1, the magnetometer data has a high contribution to the SNR improvement result. Besides the SNR improvement results, correlation coefficients between the movement artifact removed signal and the referenced ground truth signal are presented in Table 1 for both subjects 1 and 2 for each of the

movement artifact segments as another quantitative improvement indicators. This indicator signifies how much alike the signals are in respect of covariance by a single unitless quantity ranging from -1 to +1, where values closer to +1 indicates a stronger correlation between the signals [74]. For all the movement artifact segments, the correlation coefficients increase towards +1 when six channels of IMU data were used compared to only when three channels IMU data were used to estimate and remove the movement artifacts. When nine-channel IMU data were used to estimate and remove the movement artifacts, the correlation coefficients remained the same for some of the segments which is analogues to the case of SNR improvements after artifact removal from the third movement artifact segment from the first subject.

The data from the subject three and four are presented in Figure 6. In the experiments with these two subjects, the movement artifacts in the NIRS were induced by natural head movements rather than the simulated movement artifacts as presented for the first two subjects. Furthermore, the NIRS signals were converted into Oxygenated (HbO_2) and deoxygenated (Hb) hemoglobin change using Beer-Lambert law [68]. In contrast to the experiments with simulated artifacts where validation of the artifacts removal was assessed by the SNR and correlation improvement, the same validation method cannot be used in case of natural movement artifacts removal due to the lack of any reference ground truth signal. Considering that there was a minimal hemodynamic change during a short duration of the natural movement occurrence, a minimal change in concentration of the HbO_2 and Hb was used to determine the performance of the artifacts removal associated with natural movements. The result presented in figure 6 demonstrates that with additional gyroscope sensors and magnetometer, the artifact in NIRS signals can be

better removed as revealed by the minimal change of HbO_2 and Hb signals before, during, and after the movement artifacts occurred. This suggests that, in addition to the accelerometer in the IMU sensor, gyroscopes and magnetometer in the IMU are complementary to the accelerometer for a better modelling of the movement artifacts, which as a result, leads to better removal of the movement artifact in NIRS signals. A previous study [53] showed that the level of negative correlation between Hb and HbO_2 get reduced when movement occur. In the case of this study, the duration of the natural head movement resulting in artifact in NIRS signals was relatively short and hypothetically, there would not be any significant hemodynamic change during this short period. Based on this assumption, the distorted waveform of Hb and HbO_2 signals as depicted in Figure 6, was due to the artifacts contaminated in the NIRS signal. As the distorted Hb and HbO_2 waveform was due to the artifacts, the distortion should be independent of the true hemodynamic changes of Hb and HbO_2, which might be positively or negatively correlated. In the experiments performed in this study, the data showed a major negative correlation between the oxyhemoglobin and deoxyhemoglobin signal; however, after removing the distortion induced by the artifact, the level of Hb and HbO_2 kept the same as the baseline, which was in agreement with the hypothesis.

It is to be noted here, the selection of the movement artifact segments was made manually by keeping track of the time of movement artifact occurrence and later visual inspections on the raw IMU data and the raw NIRS signal. This manual detection of the segment will be automated in the future based on IMU and NIRS signal feature changes. Though this study was not purposed to evaluate the quality of the NIR signal from the custom-made system, we did perform preliminary evaluation - the raw NIRS signal was

visually inspected for the presence of a heart beating signal, showing whether the signal was correctly acquired. However, the accuracy and quality of the NIR signals using the custom-made system needs further well-controlled test, particularly, the correlation with brain functions.

Although the current results presented in this paper showed a significant improvement in artifacts removal, there are still a lot of scopes to improve the developed technique. From the system identification point of view, any movement artifact impact on the NIRS signal is unpredictable as they might differ in amplitudes, directivities, latencies, frequency contents and so on [73]; moreover, it has been observed in this research that various IMU channel might have different level of artifacts impact in different cases, which is another variability probably arise from sensor or from the nature of the artifact itself.

2.6 Conclusion

In the previous studies, the accelerometer was used in adaptive filtering for movement artifacts registering and estimating its impact in the NIRS signal. The theoretical application to accelerometer-based motion artifact removal is effective in mechanical systems, but the organic movements of a human subject are not only subjected to linear movements but simultaneous rotation and multi-directional displacements. These motions are roughly captured by the accelerometer but are effortlessly quantified with the use of the additional magnetometer and gyroscope. Thus, movement artifacts related signals detected by other sensors from IMU, along with the accelerometer signal, result in better estimation of the motion artifacts in the detected NIRS signal. In this study, the results showed that using the accelerometer, gyroscope and magnetometer signals from the IMU

sensor provide more accurate modeling of motion artifacts and thus improves the SNR improvement yields.

CHAPTER 3 SENSOR FUSION OF MOTION SENSORS

3.1 Introduction

The non-invasiveness, safety and cost-effectiveness [34] of NIRS make it an effective approach to detect blood oxygenation level. Moreover, it has been successfully employed to observe various physiological phenomena and processes [35] identifiable by blood oxygenation level, such as cardiovascular disease [36] and sepsis [37] from muscle oxygenation, cognitive involvement [16], [38] and activation of brain function [39], [40] from cerebral oxygenation. In this respect, NIRS based brain-computer interface (BCI) becoming common in the field of human-system interaction research [75]–[77] due to its certain benefits, i.e. better immunity to ambient electrical noise than conventional electroencephalogram (EEG) based BCI [78]. This interaction between humans and the system will take place outside of the lab environment in practical applications in the future. The implementations of NIRS based functional brain imaging using wearable NIRS systems in the naturalistic environment [79] promisingly indicate that NIRS based BCI [80] could be a perfect solution for human-system interaction in out of the lab situations. As this type of interaction, i.e. NIRS-BCI for gait rehabilitation [75], would incorporate body movement of a human in the loop of the systems, the improvement of detection and removal of movement artifact from NIRS signal would improve the specificity of the interactions.

In a typical NIRS acquisition system, human tissue is illuminated by near-infrared (NIR) light and a detector senses the scattered light. The subtle changes in the detected light convey the information related to the hemodynamic changes in the illuminated tissue. The changes in the detected light are so minute that it is easily corrupted by

motion artifacts, which is a very common issue with any signal acquisition from the human body. The system or human body motion, change the coupling from the skin and the NIR light source, and from the skin to the detectors [47]. These alterations of the coupling arise the motion artifacts and corrupt the NIRS signal. Although multiple sensors-based motion-sensing presented in chapter 1 showed great improvement in the estimation of motion artifacts and removal, the sensor fusion of these artifacts may further improve the accuracy of the motion sensing and, subsequently, the removal of the artifacts by improvement in the motion sensing.

3.2 Related Works

Several artifact removal techniques for NIRS have been developed in the last few decades [52]. Typical motion artifact removal techniques detect and remove abrupt changes of either frequency components or time waveform in the NIRS signal. The recent advancement in the microelectromechanical system (MEMS) chip allows for the registration of motion information during the bio-signal recording, which subsequently can be used for adaptive noise cancellation of motion artifacts. Usually, three-channel accelerometer signals have been used to estimate and remove motion artifacts from the NIRS signal in adaptive noise cancellation [64], [65]. The investigation presented in chapter 1 [81], presented that gyroscope (G) and magnetometer (M) signals along with accelerometer (A) signals from an integrated Inertia Measurement Unit (IMU), can provide a better estimation of motion artifacts in NIRS signal, and subsequently removed it from NIRS signal, when compared to the estimation using only accelerometer signals. This improvement comes from the fact that motion artifacts arise from diverse body motions, which may have better registration through the different rotational and

directional changes acquired from other sensor types, such as gyroscope and magnetometer. However, physical sensor readings suffer from imprecision, sensory deprivation, drift, and uncertainty [82]–[84]. Sensor fusion from physical sensors of accelerometer, gyroscope and magnetometer can reduce these problems in the resultant output by combining more sensor signals and may provide a more accurate estimation of the target variable, i.e., the motion artifacts in the NIR signal. This study was purposed to determine whether the combination of motion fusion algorithm-based signals and individual sensor readings from IMU could provide a more accurate correction of the motion artifacts in the NIRS signal acquired using a NIRS cyber sensor system.

3.3 Methods

3.3.1 Experimental Design and Data Acquisition

Two healthy subjects, ages 22 and 28, volunteered for this study. Six sessions of data were collected. The NIRS signals were recorded from the forehead for simplicity. During the recording, the subjects were instructed to sit comfortably. To quantify the SNR improvement of the artifact removal process, two versions of the NIRS signal were recorded from the same location using two photodiodes placed as close as possible to each other. By referring to the quantitative assessment method suggested by Sweeney's study [49], among these two versions of NIRS signals recorded using two separate channels simultaneously, one version was motion artifact-free and the other one was affected by the motion simulation. In this study, motion artifacts were simulated by tapping one of the photodiodes without affecting the other channel. The first channel reading which is unaffected by motion, is assumed to be close to ground truth signal and denoted as a "reference ground truth" signal subsequently in this study. The corrupted

NIRS signals were corrected by estimating and removing the motion artifacts in two ways, firstly using motion signal only in the artifact estimation and secondly, using motion signal as well as sensor fused signal in the artifact estimation. Afterward, SNR was calculated between the corrected NIRS signal and motion artifact-free referenced ground truth signal [49] for each version of the corrected signals and used as the quantitative measure for further assessment.

3.3.2 Motion Fusion Algorithm

Let G_x, G_y, G_z be the gyroscope readings. The sensor frame rotation in respect to the inertial frame can be expressed by the quaternion as,

$$q_\Delta = \left(\cos\left(\frac{\Delta t||G||}{2}\right), \frac{G_x}{||G||}\sin\left(\frac{\Delta t G_x}{2}\right), \frac{G_y}{||G||}\sin\left(\frac{\Delta t G_y}{2}\right), \frac{G_z}{||G||}\sin\left(\frac{\Delta t G_z}{2}\right)\right) \quad \text{Eq. 2-1}$$

With the change in rotation during one sampling period Δt, q_Δ can be updated as

$$q_{(t+\Delta t)} = q_t q_{\Delta t} \quad \text{Eq. 2-2}$$

Assuming the acceleration is small compared to the gravity and only 1g gravity is active in the inertial frame, the reflected gravity vector *F* from the inertial frame to the sensor frame is,

$$\begin{bmatrix} F_1 \\ F_2 \\ F_3 \end{bmatrix} = \begin{bmatrix} q_0^2 + q_1^2 - q_2^2 - q_3^2 & 2(q_1 q_2 - q_0 q_3) & 2(q_1 q_3 + q_0 q_2) \\ 2(q_1 q_2 + q_0 q_3) & q_0^2 - q_1^2 + q_2^2 - q_3^2 & 2(q_2 q_3 - q_0 q_1) \\ 2(q_1 q_3 - q_0 q_2) & 2(q_2 q_3 + q_0 q_1) & q_0^2 - q_1^2 - q_2^2 + q_3^2 \end{bmatrix} \begin{bmatrix} 0 \\ 0 \\ 1 \end{bmatrix} \quad \text{Eq. 2-3}$$

The difference between the reflected gravity $[F_1\ F_2\ F_3]^T$ in (3) and the accelerometer measurements $\left[A_x\ A_y\ A_z\right]^T$ can be utilized to correct the error from the gyroscope measurement drifts. To do that, the inner and the cross product of these two vectors are

calculated to get the angle ϕ and rotation axis ν of rotation error. Using this axis and angle information, the rotation error is expressed in quaternion again as,

$$q_{corrected} = q\big((1-\alpha)\phi, \nu\big) = \left[\cos\frac{\phi}{2} \;\; \nu_1 \sin\frac{\phi}{2} \;\; \nu_2 \sin\frac{\phi}{2} \;\; \nu_3 \sin\frac{\phi}{2}\right]^T = [e_0 \; e_1 \; e_2 \; e_3 \;]^T \quad \text{Eq. 2-4}$$

Finally, the quaternion can be updated as,

$$q = q_{(t+\Delta t)} q_{corrected} \quad \text{Eq. 2-5}$$

The quaternion in (5) leads to the Euler angle (Yaw, Pitch and Roll) as follows,

$$\begin{bmatrix} \theta_Y \\ \theta_P \\ \theta_R \end{bmatrix} = \begin{bmatrix} arc\tan 2(2(q_0 q_3 + q_1 q_2), 1 - 2(q_2^2 + q_3^2)) \\ arc\ \sin(2(q_0 q_2 - q_1 q_3)) \\ arc\tan 2(2(q_1 q_2 + q_0 q_3), 1 - 2(q_1^2 + q_2^2)) \end{bmatrix} \quad \text{Eq. 2-6}$$

3.3.3 Artifacts Estimation and Removal

The Autoregressive modeling with Exogenous input (ARX) was used to estimate the motion artifacts presented in chapter 1. However, the dimension *L,* which is the number of exogenous input signals used in the estimation, has changed in this investigation. Here, *L*=9 for Case 1, when using physical sensor only and *L*=12 for Case 2 physical sensors integrated with motion fusion algorithm-estimated Yaw, Pitch and Roll. $\boldsymbol{U}$ can be written for these two cases as,

Case 1: $\boldsymbol{u_1}[k] = \left[A_x[k] \; A_y[k] \; A_z[k] \; G_x[k] \; G_y[k] \; G_z[k] \; M_x[k] \; M_y[k] \; M_z[k]\right]^T$

Case 2: $\boldsymbol{u_2}[k] = \left[A_x[k] \; A_y[k] \; A_z[k] \; G_x[k] \; G_y[k] \; G_z[k] \; M_x[k] \; M_y[k] \; M_z[k] \; Y[k] \; P[k] \; R[k]\right]^T$

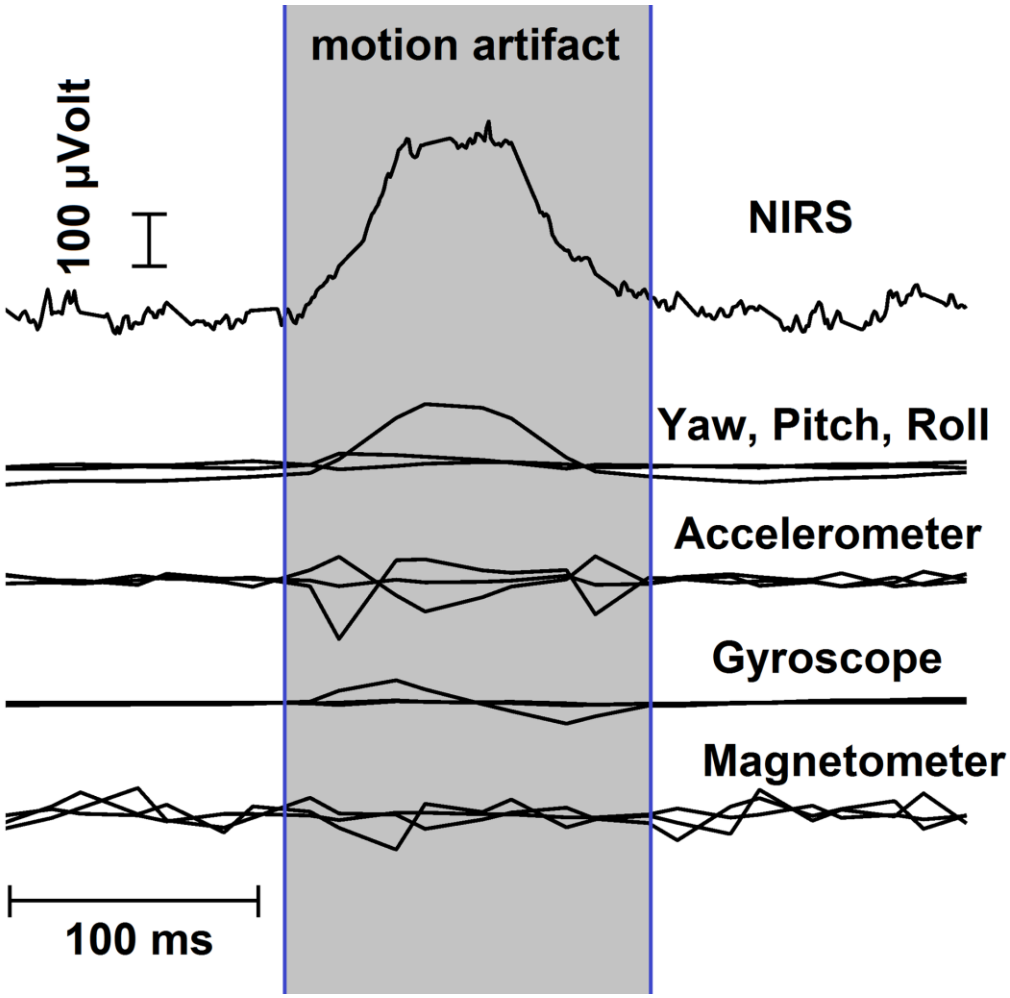

Figure 7. NIRS signal and motion signal from accelerometer, gyroscope, magnetometer and motion fusion signals (YPR).

The estimated motion artifacts $\hat{w}[n]$ is then subtracted from the signal $x[n]$ using equation (1-4) to estimate the motion artifacts free hemodynamic signal.

3.3.4 SNR Improvement Calculation

The SNR between the motion artifact corrupted NIRS signal and the referenced ground truth signal, before and after motion artifact removal, was calculated as per the equation (1-5) from chapter 1.

Table 2. SNR improvement of motion artifacts removal using sensor fusion

Motion artifact	SNR (dB) using A, G and M only	SNR (dB) using YPR fused with A, G, and M
Subject 1 segment 1	16.2	22.2
Subject 1 segment 2	17.8	18.7
Subject 1 segment 3	19.3	19.3
Subject 2 segment 1	20.6	20.6
Subject 2 segment 2	13.4	21.9
Subject 2 segment 3	9.6	10.0

3.4 Result and Discussion

Six motion artifact segments from the two subjects were analyzed in this study. Figure 7 shows the raw signal of motion artifact containing NIRS signal segment 1 from subject 1 along with the Accelerometer, Gyroscope, Magnetometer and YPR signal estimated by (6) in motion fusion algorithm. The portion of the NIRS signal shaded in gray in Figure 7 was corrupted by the motion artifacts indicated by the motion signals. Table 2 presents the quantitative result of artifacts removal for each artifact segment from each subject with respect to SNR improvement. For the first artifact segment from the first subject, a 6dB increase in the SNR was found when motion fusion signals were used in artifact estimation, and for the second segment, a 0.9dB SNR increment was found. However, there was no SNR improvement in the case of the third artifact segment from the first subject. It has already been mentioned that the sensor fusion reduces the limitations of the individual sensor's registration of the motion by combining the motion signals from multiple sensors. However, sometimes the individual sensor may perform so well that the motion fusion signal's accuracy improvement is subtle enough for the motion fusion signals to not improve the artifacts estimation accuracy. This accounts for the lack of

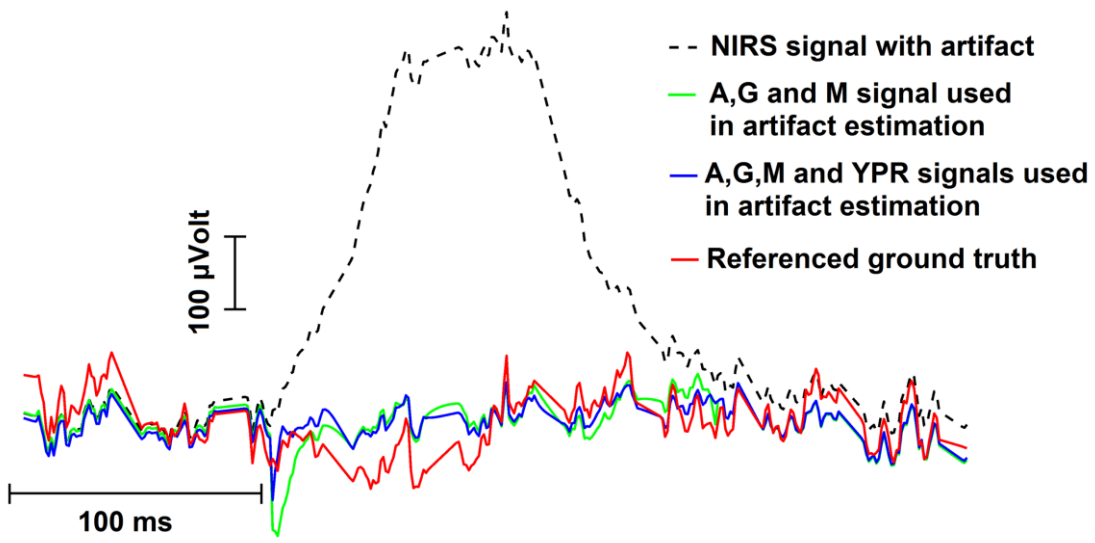

Figure 8. Qualitative result of artifacts estimation and removal process using individual sensors signal and motion fusion signals.

SNR improvement on the third segment of the first subject and the first artifact segment from the second subject is presented in Table 2. Likewise, for the remaining two artifact segments from the second subject, 8.5dB and 0.4dB SNR improvement were found.

Figure 8 shows the artifact removed NIRS signals along with the original artifacts containing the signal and the referenced ground truth signal for the qualitative assessment. The artifact-removed signal is plotted in blue, which is closer to the referenced ground truth signal plotted in red, is the result of using motion fusion signals for artifact estimation. The green line indicates the artifact-removed signal when only the conventional individual sensor signals were used in the motion artifacts estimation.

3.5 Conclusion

In this study, motion fusion was applied with individual sensor signals to increase the accuracy of the motion signals. To demonstrate this, a wearable wireless NIRS cyber sensor system was developed which incorporates an IMU sensor close to the optical

sensor to capture the motion signals along with the NIRS signal. The cyber sensor provides motion signals from three individual sensors along with the motion fused signals which are used in the estimation of the motion artifacts contribution in the detected NIRS signal. The increase in the artifact estimation accuracy due to the use of sensor fused motion signals in the estimation leads to the SNR improvement in the corrected NIRS signal. Thus, more accurate detection of the hemodynamic response would be possible which is essential for any NIRS based human in the loop system where the specificity of the signal is critical for appropriate interaction**.**

CHAPTER 4 OPTICAL SENSOR LOCATION OPTIMIZATION ON HUMAN FOREHEAD

4.1 Introduction

The invention of the wheel introduced a new role to humankind, the operator. This job requires humans to take into account the current state of the system is being operated and the current environmental situation the system is in, and then take cognitively assessed actuating commands to operate the system effectively and safely. From riding a bicycle to operating an aircraft, these jobs exert various levels of cognitive load to the operator depending on the systems. The safety of the human users accompanying the operator is highly dependent on the continuous cognitive effort of the operator, which is also denoted as the cognitive workload on the operator. For instance, a study on aviation crashes [85] based on 329 major airline crashes claimed that 38% of the crashes were probably caused due to pilot error. Thus, ensuring balanced and continuous human operator's cognitive effort via monitoring operator's cognitive workload could improve the safety of such mission-critical operations by reducing the probability of human error.

In an effort to improve safety by assessing and balancing operators' cognitive workload, subjective tests, such as [4] NASA-TLX, were used widely, which can only be done after the operator has completed the task and based on his experience during the task. The technological advancement in the modalities named as Functional Magnetic Resonance Imaging (fMRI), Electroencephalography (EEG) and Functional Near-Infrared Spectroscopy (fNIRS) in about last three decades, brings a new dimension to the cognitive workload monitoring. Now it can be even monitored while the operator is doing the task. Several studies [5], [6], [19], [86] on cognitive workloads assessment already promisingly showed that physiological signals acquired using fMRI, EEG, and fNIRS or

combination of these modalities [8], [87], which are faster than the subjective tests, can be used to monitor cognitive workloads.

The increased neural activity [2] due to the increased cognitive workload, increases the oxygen consumption in the cerebral cortex which is later regulated by the brain's control mechanism called glial regulation [3]. This blood oxygen dependent phenomena can be measured using the fMRI [12]. Although fMRI is considered as the de facto standard in detecting cerebral regional blood oxygen concentration change, the technological limitations such as huge size, high cost, high system complexity, high artifacts susceptibility, and low temporal resolution greatly reduce its usability in the out of the lab environments. On the other hand, fNIRS is a less expensive technology with higher portability, higher temporal resolution, but with a comparable result to fMRI [13], [14], [16]–[18] in the detection of local cerebral oxygenation changes, although there is some compromise of signal to noise ratio (SNR) and spatial resolution. In the case of EEG application in cognitive workload assessment [19]–[21], though it is capable of high temporal and spatial resolution, it is less portable and less immune to ambient electrical noise, which is not present in fNIRS due to its optical nature of technological implementation.

4.2 Related Works

In research of operators' cognitive workload assessment, fNIRS has successfully been used in various studies in actual or simulated environments, such as car driving [30], [88], train driving [29], and flight simulation [89]. The recent studies relating to cognitive tasks [90], [91] demonstrated that even wearable fNIRS system can detect the cognitive workload related to hemodynamic changes. Moreover, the wearability of the

fNIRS system enables such experiments being conducted in real-life scenarios, such as during walking, driving a vehicle and outdoor navigation [88], [90]–[92]. These studies are highly important in the field of engineering application utilizing the knowledge from cognitive science via fNIRS and also experimentally prove that fNIRS can be implemented in out of the lab situations. However, it's applicability and wearability can be improved if the system size can be reduced, in respect of sensing area on a human head, with retaining comparable cognitive workload detection accuracy. In other words, wearing a system on the forehead for several minutes or hours by subjects may be okay in case of experiments. However, in the case of the practical application of fNIRS on operators' cognitive workload detection during their whole day working period, the wearability of the system in respect of system dimension, weight, duration of operation on single battery recharge are the challenges to be accounted. These challenges could be mitigated if the required sensing area on the forehead could be reduced by optimizing the sensor locations for cognitive workload monitoring.

During the cognitive load, the portion of the cognitive system that retains the information for short term, necessary for processing to accomplish the cognitive tasks, is known as the working memory [93], which is widely assumed to be served by the Pre-Frontal Cortex (PFC) along with the central executive function. Several cognitive-function related studies using fMRI conform with this assumption from the observation of high hemodynamic activities in the PFC during the cognitive workloads [2], [5], [94]. This observation of regional cerebral activation during cognitive tasks leads to the implementation of fNIRS modality in assessing cognitive workload [28], [86], [95], [96] by sensing the PFC optically. In general, fNIRS based cognitive workload assessment

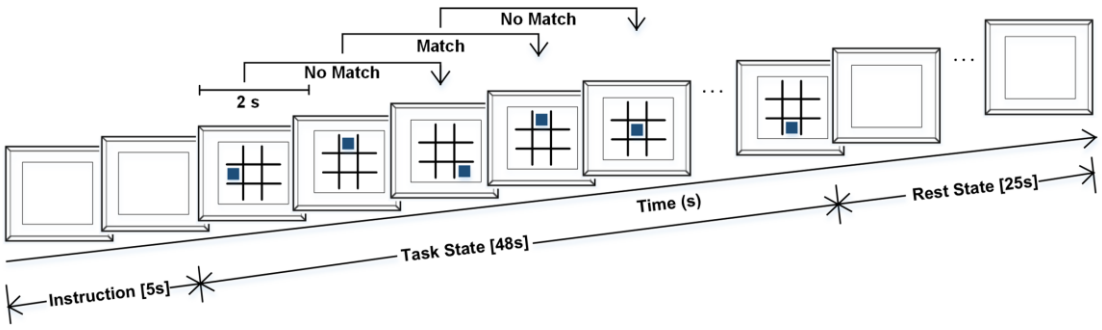

Figure 9. Positional 2-back test. Each event is 2s long and the task state lasts for 48s. Afterward, a 25s Rest state followed when the subjects did not move and visually affixed to the blank computer screen.

studies sense the whole forehead region to classify the workload, but there is not any study that answers whether it is necessary to sense the whole forehead for successful detection of cognitive workloads, or what the compromise is in the cognitive workload detection accuracy if only certain portion of the forehead is sensed.

4.3 Materials and Methods

4.3.1 Participants

Eight healthy volunteers (six males and two females) with no history of neurovascular and cognitive disorder, participated in this study. The study was approved by the Institutional Review Board (IRB-19-0091) of Florida International University and signed informed consent was obtained from all the subjects prior to the study.

4.3.2 Experimental Design

To induce the cognitive workload in human subjects, the n-back task is widely used [86], [87], [94] paradigm related to cognitive study in research, which was first demonstrated by Kirchner WK. [97]. In this paradigm, the subject observes some series of events during the testing period and if any of the events match with n-events before then the subject provides feedback, where n could be 1,2,3 and so on depending on the

requirement. As the target of this study is to explore how the detection accuracy of cognitive workload varies due to the sensing location on the human forehead, a moderate level of cognitive workload induction was applied, which is assumed to be the 2-back test. A free open-source software [98] named "Brain Workshop" was used to simulate the positional 2-back task, where a solid colored square changed its position randomly within a 3 by 3 grid in every two seconds (Figure 9 depicts this task paradigm). If the current position of the square matched with its position 2 events before, the subject pressed a button on the keyboard and did nothing if the position did not match. In each session of recording, there were 24 events of the positional 2-back task, which spanned 48 seconds and afterward 25 seconds of relaxing when subjects did nothing. This relaxing period was considered as the Rest state [87]. Recording of each session starts 10 seconds prior to the start of the 2-back task which was used as the baseline of the diffused optical signal in the conversion of the absorption of optical signals to hemodynamic change. Each subject did 10 of such sessions where the subjects relax for about 30 seconds between the sessions and during this period data was not recording and the subjects were free to move. The sessions with less than 90% accuracy in 2-back task performance were rejected during the recording.

4.3.3 Data Acquisition and Signal Processing

A wearable wireless fNIRS system developed by the Human Cyber-Physical Systems Lab at Florida International University was used for data acquisition in the experiment. The system architecture was based on the sensor system developed in [70], [81], and modified to accommodate more channels required to sense the whole forehead. The improved system consists of three light-emitting diodes (LED) as a source of near-

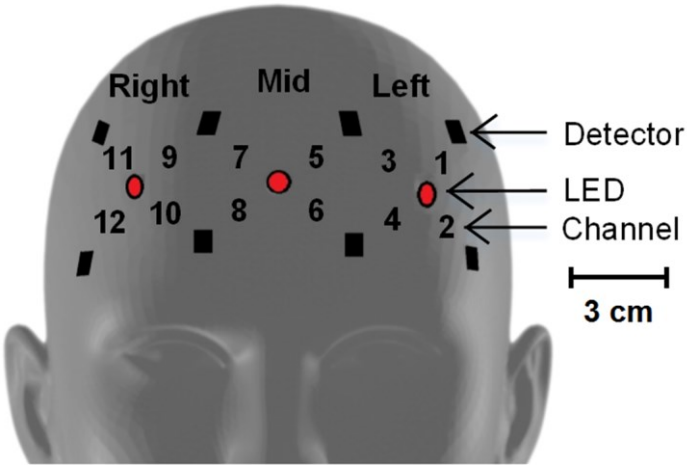

Figure 10. Photodetector placement and channel positions. All the distances between detector and LED are same and 3 cm. The distance between adjacent detectors are 5.5cm horizontally and 4.5cm vertically. Similarly, the distance between adjacent LED is 5.5cm.

infrared (NIR) light capable of multiwavelength (770nm and 850nm) emission and eight photodetectors (PD) as light detectors, where the source-detector distance is 3 cm with 0.3 cm variability. The LED and PD together form twelve channels for sensing which are marked by channel numbers in Figure 10. The system covers the whole forehead for sensing which is the region of interest (ROI) in this study. This ROI is subdivided into five sub-location named as Left, Mid, Right, Left-Mid and Right-Mid. The channels 1 to 4 sense the left location on the forehead, the channels 5 to 8 sense the mid location on the forehead and the remaining channels 9 to 12 sense the right location on the forehead. The location stated by Left-Mid and Right-Mid consist of channels 1 to 10 and channels 3 to 12, respectively. The location name for the whole forehead sensing area is indicated by the name Whole in subsequent descriptions. Each channel was sampled at 25Hz sampling rate. Additionally, the headband that houses the system is equipped with a nine-channel inertial measurement unit (IMU) and record the movement data concurrently with NIR data. IMU data were checked immediately after each session from each subject for movements during the recording and the sessions that showed movements were

discarded. The raw NIR signals were low pass filtered with third-order Butterworth bandpass filter with 0.01 – 0.5 Hz cut-off frequency [99], and afterward, a two-second windowed moving average filter was applied to further remove any physiological interference in the detected NIR signal, such as Mayer wave, respiration and heart rate [100], [101]. Afterward modified Beer-Lambert [68] law was applied to convert the multiband raw NIR signal to oxygenation change signals, known as the change in oxygenated hemoglobin (ΔHbO_2) and deoxygenated hemoglobin (ΔHbR).

To study how the workload detection accuracy varies with the length of sensing period along with the sensing location on the forehead, the oxygenation change signals were segmented with various window lengths, such as 5, 10, 20, 25 and 48 seconds [87]. There was about 50% overlap [87] in the windowing when the segmentation window length was less than the whole period of the 2-back or Rest state. The overlapping is assumed to be necessary to reduce inter-subject variability in statistical temporal features of the signal [87], [102]. After segmentation, each signal segment was labeled as 2-back or Resting-state accordingly.

This segmentation process resulted in n segments of 2-back state signal and m segments of resting-state signals. Here the values of n and m were dependant on the segmentation window lengths used in this study. For each session of any subject, it resulted in (n , m)=(18 , 11) when segmenting with 5 seconds window, (n , m)=(9,5) for 10 seconds window, (n , m)=(4,2) for 20 seconds window, (n , m)=(2,1) for 25 seconds window and (n , m)=(1,1) when using whole period of the each state. These values of n and m also signify the number of samples in each class at different segmentation window lengths. All sessions of each subject, after segmentation and appropriate class label

assignment, resulted in 290, 140, 60, 30 and 20 samples for the segmentation window lengths of 5, 10, 20, 25 seconds and whole state period, respectively.

4.3.4 Feature Extraction

From each segmented hemodynamic change signal sample, commonly used statistical features were extracted, such as mean [103], [104], variance[105], slope [103], [104] of polynomial fit, skewness [105], [106], kurtosis [105], [106] and correlation [87] of ΔHbO_2 and ΔHbR. These features extraction from each channel resulted in a total of 11 features per channel for any samples under any segmentation window length. As there were various numbers of channels were involved in sensing different locations on the forehead, various numbers of features resulted from each sample depending on the sensing location on the forehead. For example, there were 44 features for Left, Mid and Right location whereas there were 110 features for Left-Mid and Right-Mid Location for any length of segmentation. As there were 12 channels involved in the whole forehead location, there were 132 features resulted for the location denoted by Whole.

4.3.5 Feature Selection and Classification

In case of fNIRS based classification problem, several classification methods have been used, such as Discriminant analysis (DA) [77], [106], Support Vector Machine (SVM) [107]–[112], Artificial Neural Network (ANN) [113]–[116] and so on. As the pivotal point of the study was to assess the cognitive workload monitoring accuracy variability using wearable fNIRS upon various sensing locations on the forehead, the speed of the classifier was a crucial property in consideration. Thus, the Linear SVM, which was already used in several other fNIRS based classification studies [87], [107], [117], was selected as a classifier in this study. In this respect, the generic

implementation of Linear SVM in MATLAB platform with box constraint of 1 and auto kernel scale was used for classification. For feature selection, two algorithms were used, namely Sequential Forward Selection (SFS) Wrapper algorithm [118] for feature subset selection and Relief algorithm [119], [120]. Each of these algorithms has its own merits in respect of the statistical relevance (Relief) of the features to the classes [119] and the interaction of the training feature set (SFS) with the classifier algorithm [118]. Thus, both of the selected feature-sets returned by these two algorithms were individually used in the classification using the linear SVM. The best accuracy among these two classification results was used in the statistical analysis. In this respect, as the SFS claims to return optimal feature subset by heuristic search, the whole subset of the returned features was used in classification. On the other hand, as the Relief algorithm instead returns the ranks and weights for all the features, only the features with positive weights were used in the classification.

In the classification process, ten-fold testing cross-validation was applied [121]–[123]. In other words, there were 240 datasets resulting from segmentation, and in each of the classification process on these datasets, the dataset was partitioned into ten subsets using a random selection of the observations for each partition. Then, the SVM was trained using the nine subsets of this dataset leaving out the remaining one subset for testing. This leave-out subset is never seen by the classifier during the training phase. The training of the SVM was done using ten-fold training cross-validation using those nine subsets of the partitioned data. Afterward, the trained SVM classifier was used to test the classification accuracy using the subset not used in training. Subsequently, this same training and testing procedure was applied on the other remaining nine subsets of this

dataset in a way nested cross-validation. The final accuracy of the classification on this dataset was calculated as the mean accuracy of these ten testing accuracies.

4.3.6 Statistical Analysis

For all the eight subjects, cognitive workload classification accuracies were calculated on the sensing locations Left, Mid, Right, Left-Mid, Right-Mid, and Whole, under several segmentation windows. The mean classification accuracies for each location across all the subjects were different from each other. Thus, to find the statistical significance of the differences in the mean classification accuracies of all subjects for each location (Left, Mid, Right, Left-Mid, Right-Mid) with the accuracy of the whole forehead location (Whole), two-sample t-test was applied with 5% significance level, which return the test decision whether the means are statistically equal or not at that significance level.

4.4 Results and Discussion

All the classification accuracies from all the datasets are presented in Table 3. For the 5-seconds segmentation window, the lowest mean accuracy for all subjects was 83.4% with a standard deviation of 6.7%, which resulted when only the Right location was used. On the other hand, the highest mean accuracy resulted when the Whole forehead dataset was used to classify, which was 94.0% with a 3.9% standard error. Like 5-seconds segmentation window, the Right location in all other segmentation windows also resulted in the lowest classification accuracies, which were 84.0%, 86.5%, 90.8% and 95.0% for 10, 15, 20, 25- and 48-seconds window length, respectively. For the 48-seconds segmentation window, the Left location also resulted in the lowest classification accuracy like the Right location but with a higher standard deviation which was 6.5%. In case of

Table 3. Classification accuracies along with mean and standard deviation (SD) across all subjects for each location on the forehead.

		Classification accuracy (%)					
		Left	Mid	Right	Left-Mid	Right-Mid	Whole
05s window	Sub1	82.4	88.3	84.5	89.3	89.0	92.1
	Sub2	87.2	95.5	80.0	98.3	97.6	98.6
	Sub3	80.0	87.2	72.1	87.2	90.0	91.4
	Sub4	84.1	76.9	85.2	83.8	85.2	89.3
	Sub5	94.1	92.1	93.1	96.9	99.3	98.6
	Sub6	91.4	97.9	87.6	96.2	96.9	98.3
	Sub7	90.0	88.9	87.9	92.4	93.4	93.1
	Sub8	78.3	84.1	77.2	90.7	88.3	90.3
	Mean ± SD	85.9 ± 5.7	88.9 ± 6.6	83.4 ± 6.7	91.9 ± 5.0	92.5 ± 5.1	94.0 ± 3.9
10s window	Sub1	82.9	92.1	85.0	91.4	89.3	91.4
	Sub2	88.6	94.3	90.7	98.6	93.6	99.3
	Sub3	79.3	70.7	72.1	86.4	89.3	81.4
	Sub4	89.3	75.0	80.0	86.4	90.7	85.7
	Sub5	94.3	91.4	96.4	97.1	99.3	97.9
	Sub6	91.4	97.9	85.0	97.1	97.9	98.6
	Sub7	90.7	92.2	82.2	93.6	94.4	92.7
	Sub8	84.3	87.1	80.7	87.9	90.0	91.4
	Mean ± SD	87.6 ± 5.0	87.6 ± 9.6	84.0 ± 7.3	92.3 ± 5.0	93.0 ± 3.9	92.3 ± 6.3
20s window	Sub1	86.7	95.0	83.3	88.3	90.0	93.3
	Sub2	93.3	100.0	93.3	98.3	95.0	95.0
	Sub3	83.3	81.7	70.0	86.7	85.0	85.0
	Sub4	93.3	70.0	86.7	91.7	93.3	90.0
	Sub5	98.3	98.3	93.3	98.3	100.0	100.0
	Sub6	96.7	100.0	90.0	96.7	96.7	93.3
	Sub7	86.6	94.7	85.2	95.2	94.7	95.2
	Sub8	88.3	93.3	90.0	93.3	88.3	93.3
	Mean ± SD	90.8 ± 5.4	91.6 ± 10.5	86.49 ± 7.6	93.6 ± 4.4	92.9 ± 4.8	93.2 ± 4.3
25s window	Sub1	100.0	93.3	83.3	96.7	100.0	100.0
	Sub2	96.7	100.0	96.7	100.0	100.0	100.0
	Sub3	90.0	83.3	76.7	83.3	80.0	83.3
	Sub4	93.3	86.7	90.0	93.3	93.3	90.0
	Sub5	100.0	100.0	100.0	100.0	100.0	96.7
	Sub6	86.7	100.0	93.3	100.0	100.0	100.0
	Sub7	96.7	96.7	96.7	97.5	96.7	93.3
	Sub8	93.3	90.0	90.0	96.7	93.3	90.0
	Mean ± SD	94.6 ± 4.7	93.8 ± 6.5	90.8 ± 7.7	95.9 ± 5.6	95.4 ± 6.9	94.2 ± 6.1
48s window	Sub1	100.0	100.0	90.0	100.0	100.0	100.0
	Sub2	95.0	100.0	95.0	100.0	100.0	100.0
	Sub3	85.0	90.0	90.0	95.0	90.0	90.0
	Sub4	100.0	90.0	95.0	100.0	95.0	100.0
	Sub5	100.0	100.0	100.0	100.0	100.0	100.0
	Sub6	85.0	100.0	95.0	100.0	100.0	100.0
	Sub7	95.0	90.0	100.0	96.7	95.0	95.0
	Sub8	100.0	95.0	95.0	95.0	100.0	100.0
	Mean ± SD	95 ± 6.5	95.6 ± 5.0	95 ± 3.8	98.3 ± 2.4	97.5 ± 3.8	98.1 ± 3.7

highest mean accuracy of classifications beyond the 5-seconds segmentation window length, Left-Mid location yielded highest mean accuracy for 20, 25- and 48-seconds

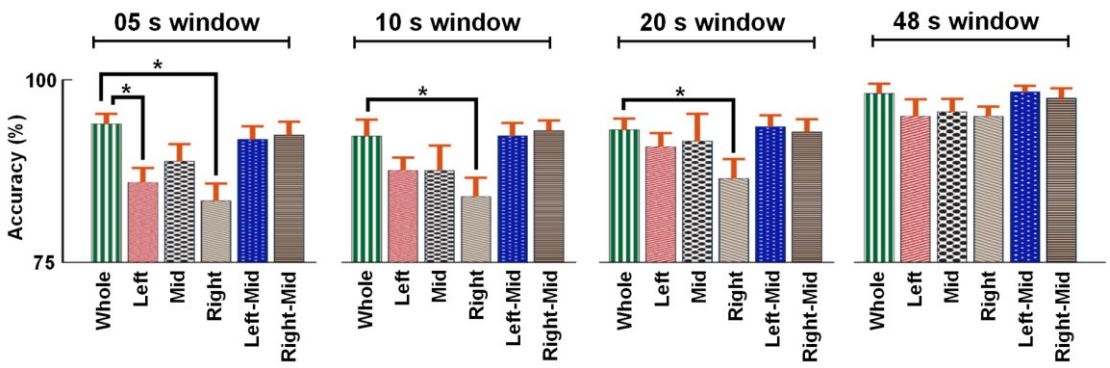

Figure 11. Mean accuracy of classifications across various location for different segmentation window length. The Standard errors of the mean classification accuracies are presented by the errorbars. The four classification accuracies mean whose differences are statistically significant, are presented by the significance-link with the star.

segmentation window lengths which are 93.6%, 95.9 and 98.3% respectively, and for the remaining 10-seconds segmentation window length Right-Mid resulted in highest mean accuracy of classification which was 93.0%.

Regarding the statistical analysis aforementioned, two-sample t-test was used to test the statistical significance of the differences in the mean classification accuracies for each location (Left, Mid, Right, Left-Mid, Right-Mid) to the whole forehead location denoted by Whole. The t-test hypotheses testing decisions indicated that the mean classification accuracies were statistically different from the mean classification accuracy of location Whole in case of only in 10- and 20-seconds segmentation window lengths at location Right and in 5 seconds segmentation window length at locations Left and Right. In other words, except for these four cases, the mean classification accuracy for any location or segmentation window lengths, statistical significance was not found for the difference in the mean classification accuracies. Moreover, these results indicate that the Mid location, which is one of the three smallest sensing locations (Left, Mid, Right), resulted in mean classification accuracy with a statistically insignificant difference, compared to the largest location Whole for any segmentation window lengths.

The mean classification accuracies have been depicted by the bar plot in Figure 11 for a qualitative assessment of how the classification accuracies vary along with the increase of the sensing location on the forehead, which are grouped into segmentation windows. The error bars in the plot show the standard error of the mean accuracies, which was estimated by dividing the standard deviation by the square root of the number of subjects in this study. From this plot, it is apparent that the differences in the mean accuracies between the largest location Whole to the other smaller locations get reduced with the increase of segmentation window length.

Optical methods, such as fNIRS, which can reach a depth of few centimeters only from the skin of the human brain, could only sense hemodynamic changes of the brain tissue which are closer to the cerebral surface, such as PFC under the forehead. PFC is one of the most functionally correlated subsystems [124] among other cerebral subsystems such as Hippocampal Formation (HF), Inferior Parietal Lobule (IPL) and so on, which form the default network in respect of cognitive states. Moreover, researches based on other methods such as fMRI, Positron Emission Tomography (PET), showed the Medial PFC in this network is the most involved region on the PFC related to the cognitive states [125]. In congruence with those physiological study-based findings, the statistical result presented in this study also showed that sensing the Mid location only can result in significant accuracy in cognitive workload classification compared to the location Whole on the forehead. Thus, from the system design point of view, the fNIRS system could be minimized to sense only Mid location on the forehead with statistically insignificant compromise of the cognitive workload detection accuracy. Alike Mid location, the other two smallest sensing locations, Left and Right, could also be targeted

for cognitive workload detection using minimized fNIRS system but with higher latencies in getting significantly comparable accuracy.

4.5 Conclusions

Statistically significant classification accuracy of cognitive workload can be achieved by sensing on the Mid location on the human forehead rather than the whole forehead using fNIRS. Thus, wearable wireless fNIRS systems which are resource and power constraint by nature, can be improved by minimizing the system design with optimized sensor locations on the forehead for cognitive workload monitoring.

CHAPTER 5 VIGILANCE DETECTION DURING GAIT

5.1 Introduction

It has been showed in other studies that fNIRS signals are susceptible to motion artifacts [52], [126]–[128]. Consequently, it can be hypothesized that vigilance level detection will be altered by the motion artifacts arise from the gait. Moreover, successful removal of these artifacts may improve the detection accuracy of the vigilance level during human locomotion. Although there are several studies carried out to detect brain activations related to dual-tasking involving walking as one of the tasks [129]–[132], it has not been investigated whether the vigilance level distinguishability during walking is impacted by the walking associated motion artifacts or not. Moreover, even if it is distinguishable from the motion artifacts impacted brain signals, the question of whether this distinguishability in the walking state differs from the distinguishability to the sedentary state vigilance level detection remains unanswered.

The purpose of the study was to investigate the effect of motion artifacts on vigilance level detection while walking. Additionally, it was also explored whether a similar vigilance detection performance could be achieved during walking compared to the seated state. To achieve these goals, an experimental protocol was designed to induce different vigilance levels during walking and seated states. A supervised classification method was employed to detect the vigilance levels in both conditions from brain hemodynamic signals. The vigilance detection accuracies thus obtained were compared to assess the effect of motion artifacts on vigilance detection performance. The comparison implied that the motion artifacts reduce the vigilance level detection performance for the walking state. Afterward, motion sensor signals based artifacts

estimation and removal method was implemented to explore whether an enhancement in vigilance level detection performance could be achieved by removing artifacts or not.

5.2 Related Works

There are several studies conducted to explore human brain dynamics during walking. The target of most of the studies to detect the hemodynamic change during walking compared to resting state [133]–[135]. The results of those reveal the increase of fNIRS activity in several brain regions during walking such as the prefrontal cortex, premotor cortex, supplementary motor area, primary motor area and primary somatosensory cortex. Holtzer et al. reported increased PFC signal during walking and cognitive tasks among young and old subjects [136]–[138]. However, Lin et al. found decreased PFC activity in similar study in young subjects [129]. While these studies demonstrated the detectability of the brain dynamics during walking, it was not investigated whether the level of vigilance is detectable of not from the change in the fNIRS signals.

5.3 Materials and Methods

5.3.1 Participants

Nineteen healthy volunteers (six females and thirteen males) with no history of neurovascular and cognitive disorder participated in this study. The study was approved by the Institutional Review Board of Florida International University and signed informed consent was obtained from all the subjects prior to the study.

5.3.2 experimental design

Inducing a specific level of vigilance or cognitive workload in humans is impossible to guarantee. However, there are some widely accepted methods to use in experimental

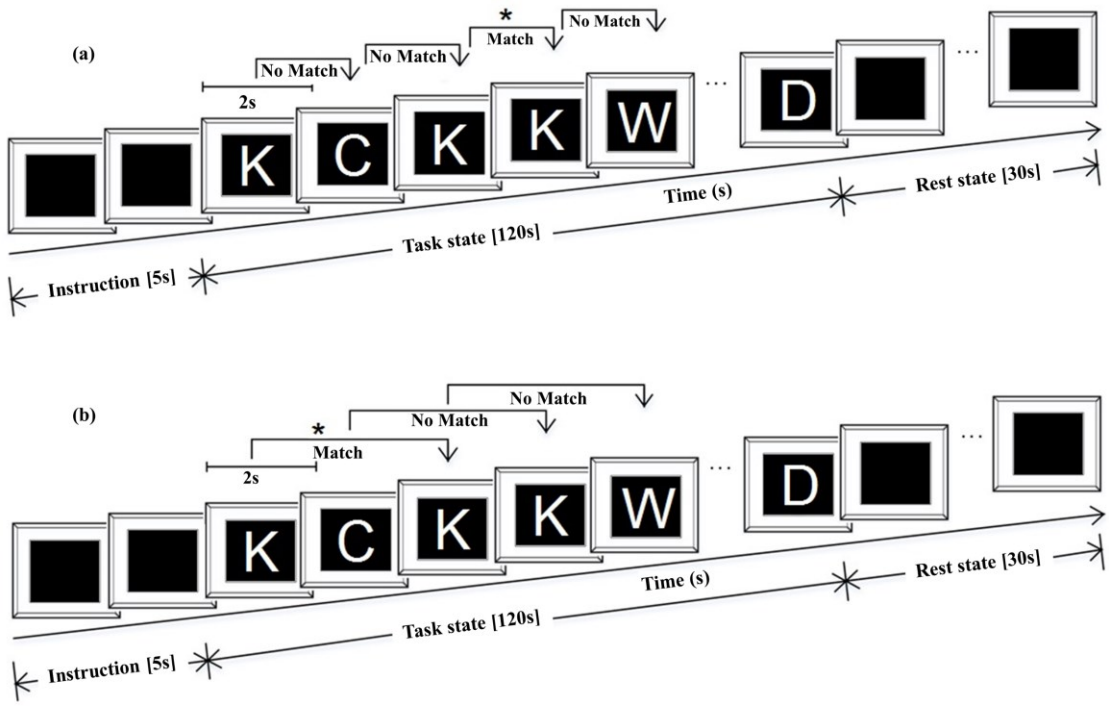

Figure 12. n-back trials. Each event is 2s long and the task state lasts for 120s. Afterward, a 30s Rest state followed when the subjects did not move and visually affixed to the blank computer screen. (a) 1-back and (b) 2-back.

design, which hypothetically entails the subject to put different levels of cognitive efforts. The n-back task is one such paradigm [86], [87], [94], which was first demonstrated by Kirchner WK. [97]. In the n-back task paradigm, the subject is presented with a series of events and if any of the events match with n-events before then the subject provides feedback. As this task require the subject to pay continuous attention towards surrounding for specific targets [1], take an executive decision upon target match [139] and execute the motor function to give response upon target match, we assume this task phenomenon closely resembles a person doing vigilance task in a field. There are several values of n in the n-back task, such as 0,1,2,3 and so on. Here, the higher the value of n in the n-back task, the higher the cognitive effort the subject has to provide to achieve a certain level of accuracy on the task. In this study, 1-back and 2-back task were used to

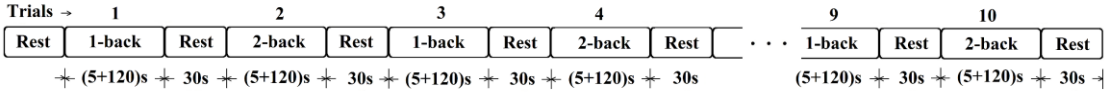

Figure 13. Timing of each n-back tasks and resting state in each of the two sessions. In session 1, the subject did 10 n-back trials while seated on a chair and in session 2, the subject did 10 n-back trials while walking on a treadmill at a preferred speed.

induce low and high cognitive workload in the subject, respectively. A sequence of English letters was selected as the n-back event in this study which is depicted in Figure 12.

Each subject participated in two sessions of n-back tasks. In each of the sessions, the subject did ten n-back tasks whose sequence and timing are depicted in Figure 13. Each n-back trial in each session spanned 120 seconds and each n-back event lasted for 2 seconds each and prior to starting, there was a 5 seconds instruction of which n-back was going to start. There was a mandatory resting period of at least 30 seconds between two consecutive n-back trials when the subjects did not move and visually affixed to the blank computer screen. Recording of each session starts 30 seconds prior to the start of the first n-back task. This portion of the signal was used as the baseline of the diffused optical signal in the conversion of the absorption of optical signals to hemodynamic change.

During the first session, the subject did the n-back tasks while seated on a comfortable chair. In the second session, the subject did the n-back tasks while walking at a preferred walking speed. Additionally, at the end of the walking session, two portions of about 20s long signal were recorded while the subject was instructed to just walking without doing any vigilance task. These two portions of the signals were used in artifacts estimation in later processing. There was a mandatory resting period of at least 10 minutes between these two seated and walking sessions.

The n-back tasks were implemented using the software "Psychology Experiment Building Language(PEBL) and Test Battery" [140]. The sequence of the English letters as the n-back event in this study was presented on three monitors simultaneously. The monitors are placed at about 0°, -60° and 60° angle to the sagittal plane of the subject. During the seated session, the subject was instructed to look at only the monitor at 0° and during the walking session, the subject was instructed to look at different monitors at different times. Moreover, there was a light-emitting diode (LED) placed on each monitor to indicate the subject to look at that monitor when it is on. These LEDs were turned on by a controller one at a time and the selection of which LED to turn on was programmed by a random number generator. This randomly looking at different monitors while doing the task assumed to make better emulation of vigilance tasks while walking. To provide a response during the n-back task, the subject used a handheld wireless button. The PEBL software assesses the objective performance of the subject based on the responses during the task. The n-back task performance accuracy is measured as the fraction of the correct responses where the missed target was also considered as an incorrect response. The acceptable n-back task performance level was set at >80% for the 1-back task to consider the subject attentive enough for the study [87].

5.3.3 Data acquisition

For the data acquisition in the experiment, A wearable wireless fNIRS system developed by the Human Cyber-Physical Systems Lab at Florida International University was used. The system is capable of recording 12 channels of fNIRS signals and it was developed based on the system architecture presented by Wang et al. [70], [141]. The system consists of three light-emitting diodes (LED) as a source of near-infrared (NIR)

light capable of multiwavelength (770nm and 850nm) emission and eight photodetectors (PD) as light detectors. The source-detector distance of the system is 3 cm with 0.3 cm variability. These LED and PD were multiplexed in the signal sensing algorithm to act as 12 channels of fNIRS for sensing the PFC. Each channel of the system was sampled at 25Hz. Additionally, the headband that houses the system is equipped with 2 six-channel inertial measurement unit (IMU) and record the movement data concurrently with NIR signals.

5.3.4 Signal Processing

5.3.4.1 ARX modeling and artifacts removal

The ARX modeling presented in chapter 1 was used to estimate walking-related movement artifacts $w[n]$ in the detected signal $s[n]$. Although LS returns the best model coefficients to fit the training signal for specific order Na and Nb, artifact estimation from the validation signal using the trained ARX model varies due to overfitting or underfitting. To select the best orders, the signal to noise ratio (SNR) of the artifact removed validation signal was assessed using the non-walking fNIRS signal as the reference signal. SNR improvement was determined as follows[71],

$$\Delta SNR = 10\, log_{10}^{\left(\frac{\sigma^2_{non-walking}}{\sigma^2_{walking_{after}}}\right)} - 10\, log_{10}^{\left(\frac{\sigma^2_{non-walking}}{\sigma^2_{walking_{before}}}\right)} \quad \text{Eq 5-1}$$

From the ΔSNR improvement values for various combinations of Na and Nb, the best combination of the model order Na and Nb was selected which reflects the highest ΔSNR on validation signal. This best order combination was then used to train an ARX model using the training signal and afterward, this trained model was used to estimate

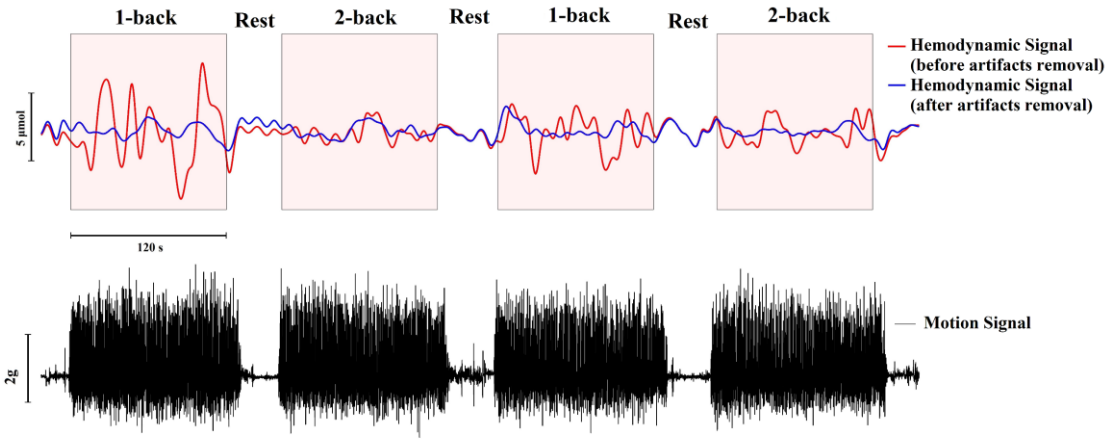

Figure 14. A representative portion of MBLL converted hemodynamic signal from walking state fNIRS signal and artifacts removed version of the same hemodynamic signal.

motion artifact $\hat{w}[n]$ in the validation signal. This estimated motion artifact was used to estimate the motion artifact removed hemodynamic signal $\hat{s}[n]$ using as per the equation (1-4). This method of ARX modeling and artifacts estimation was applied on each channel of fNIRS signals for each subject.

5.3.4.2 Conversion to hemodynamic signals

To remove physiological interference in the detected NIR signal, such as the Mayer wave [100] and heart rate, the raw NIR signals were high pass filtered with a fourth-order Butterworth filter with 0.01 Hz cut-off frequency [99]. Afterward, filtered with a fourth-order Butterworth low pass filter with 0.14 Hz cut-off frequency [142].

Afterward, modified Beer-Lambert [68] law (MBLL) was applied to convert the multiband raw NIR signal to oxygenation change signals, known as the change in oxygenated hemoglobin (ΔHbO_2) and deoxygenated hemoglobin (ΔHbR). As a qualitative representation of the effectiveness of the motion artifacts removal algorithm, a portion of the MBLL converted raw fNIRS signal with and without artifacts removal has been depicted in Figure 14.

5.3.4.3 Signal segmentation and feature extraction

The oxygenation change signals were segmented with 2 seconds window length. There was a 50% overlap [87] in the windowing during the segmentation. The overlapping is assumed to be necessary to reduce inter-subject variability in statistical temporal features of the signal [87], [102]. After segmentation, each signal segment was labeled as 1-back or 2-back state accordingly. This segmentation process resulted in 595 segments of 1-back state signals and 595 segments of 2-back state signals for each subject in each session.

From each segmented hemodynamic change signal sample, commonly used statistical features were extracted, such as mean [103], [104], variance[105], [112], slope [103], [104] of polynomial fit, skewness [105], [106], kurtosis [105], [106] and correlation [87] of ΔHbO_2 and ΔHbR. These features extraction from each channel resulted in a total of 11 features per channel for any samples of any state. As there were 12 channels in total, there were 132 features resulted from each sample.

5.3.5 Feature selection

For feature selection, "Select from Model" was used in this study. In this method, a classifier is initially trained with all the features in the training dataset. In this respect, the chosen classifier should calculate the importance of each of the features based on the feature value distributions which makes the classes most separable. For instance, in this study, an "Extra Trees Classifier" was used as the basis of feature selection [143]. In Extra Trees Classifier, the features are given importance values based on the normalized total reduction in the Gini index using a set of de-correlated random forest type classifiers. This importance value is termed as Gini importance. Afterward, features were

selected based on the Gini importance returned by the trained model. For that purpose, the features were sorted in descending order according to the returned Gini importance score for a training dataset. From the sorted list of the features, the top 12 features were selected to be used for the next steps in the classification process. In any supervised learning, feature selection is a general step to optimize the result of the classification process. It helps in reducing the number of features in the feature set by removing less correlated feature to the classes.

5.3.6 Classification

In the classification process, four-fold testing cross-validation was applied. In other words, each dataset was partitioned into four subsets using a random selection of the observations for each partition. Then, feature selection and training of a classifier were done using the three folds of the dataset. Afterward, testing was done using the remaining one-fold of the dataset. The same training and testing process was applied on the remaining three folds as well and the final accuracy of the classifications was reported as the mean of the four testing accuracies. This overall classification process was initially performed on a small subset of the dataset. The Linear Discriminant Analysis (LDA) was used to investigate whether the dataset is linearly separable or not, though LDA is generally used for dimensionality reduction in the classification process. Afterward, the classifiers, namely Support Vector Machine (SVM), k-Nearest Neighbors (KNN) and Gradient Boosting Classifier (GBT) were selected in search of a best-suited classifier for the binary classification problems in this study. All the classifiers were tuned for optimized hyperparameters using grid-search in Scikit-learn [144] to ensure the

Table 4. Behavioral task performance.

	Seated		Walking	
	1-back	2-back	1-back	2-back
Sub 1	94.75	92.25	94.10	87.74
Sub 2	96.06	88.06	93.11	80.97
Sub 3	96.39	92.26	85.57	88.06
Sub 4	98.69	92.10	99.02	94.20
Sub 5	99.34	92.58	98.36	94.52
Sub 6	97.38	84.52	91.15	87.10
Sub 7	96.72	87.42	94.10	86.77
Sub 8	97.70	90.97	94.75	88.06
Sub 9	96.72	90.00	98.77	92.14
Sub 10	98.03	85.16	95.41	83.87
Sub 11	96.07	90.65	97.70	92.26
Sub 12	97.70	86.13	97.38	85.48
Sub 13	93.44	89.03	93.44	90.00
Sub 14	99.02	87.74	96.31	93.01
Sub 15	97.05	93.87	96.39	92.26
Sub 16	100.00	85.48	98.69	88.06
Sub 17	95.08	88.39	92.46	90.65
Sub 18	97.38	86.77	98.69	93.23
Sub 19	99.67	96.45	98.69	98.06
Mean	97.22	89.46	95.48	89.81

optimized performance of each classifier for the dataset. Afterward, the classifier with the best accuracy score among them was selected in the further classification process.

5.3.7 Statistical analysis

The mean classification accuracy of the vigilance for all subjects was highest for the seated state and lowest when the task was done while walking. The classification accuracy got improved when artifacts removal was applied to the walking state dataset. Although optimization of the hyperparameters ensures the optimum classification accuracy, this improvement in the mean classification accuracy does not reflect whether it is intrinsic to the distribution of the datasets or not. Therefore, there must be a statistical analysis to evaluate the significance of the obtained improvement in classification

Table 5. Performance of various types of classifiers in vigilance detection of seated state for five subjects.

	LDA	SVM	KNN	GBT
Sub 1	58.49	52.27	62.79	89.16
Sub 2	55.46	48.90	74.74	92.44
Sub 3	54.29	57.06	66.13	90.92
Sub 4	62.61	47.98	69.08	85.72
Sub 5	58.32	47.98	90.27	93.61

accuracy. To find the statistical significance of the differences in the mean classification accuracies of all subjects during walking compared to the seated state, a two-sample t-test was applied with a 5% significance level, which returns the test decision whether the means are statistically equal or not at that significance level.

5.4 Result and Discussion

The behavioral task performances of each subject during seated and walking in this study are presented in Table 4. The maximum and minimum task performances for the 1-back task during seated were 100% and 93.4% respectively whereas, during walking, the performance was 99.02% and 85.6% respectively. On the other hand, for the 2-back task, the maximum and minimum performances were 96.5% and 84.5% for the seated state, respectively and for the walking state, it was 98.06% and 81.0%, respectively. No subject was rejected as the lowest 1-back task performance was 85.6% among all the subjects, which is higher than the threshold of 80% for the 1-back task set at the beginning of the study. In the study conducted by Lin et al. [129], which employed human walking and cognitive task, they didn't find any correlation of behavioral outcomes to hemodynamic change. Although the metric used in this study is different, alike that study, we didn't find any correlation among the behavioral outcomes and the classification accuracy in any of the seated or walking state cognitive workload detection in this study.

Table 6. Classification accuracies along with mean and standard error (SE) across all subjects for seated state, walking state and walking state with artifact removal.

	Seated	Walking (*without removal of artifacts*)	Walking (*with removal of artifacts*)
Sub 1	89.16	87.65	88.82
Sub 2	92.44	87.73	91.34
Sub 3	90.92	88.48	90.42
Sub 4	85.72	82.86	84.29
Sub 5	93.61	90.84	91.60
Sub 6	92.69	80.68	81.85
Sub 7	84.96	92.01	92.43
Sub 8	89.16	85.04	84.79
Sub 9	92.27	88.07	87.65
Sub 10	91.93	91.01	91.18
Sub 11	87.06	83.87	86.89
Sub 12	91.60	87.73	87.99
Sub 13	89.07	86.05	87.73
Sub 14	91.69	91.60	91.77
Sub 15	89.75	86.64	85.80
Sub 16	86.89	86.05	87.82
Sub 17	90.76	83.61	88.49
Sub 18	85.29	80.08	83.28
Sub 19	80.17	73.53	72.61
Mean ± S.E	89.22 ± 0.79	85.98 ± 1.05	87.2 ± 1.08
t-Test (p)		0.0183	0.1370
t-Test (h)		1	0

As mentioned earlier, initially, a small subset of the dataset was used to assess various types of classifiers' performance in vigilance detection. In this regard, seated state vigilance data of five subjects were evaluated using LDA, SVM, KNN and GBT. The results presented in Table 5 indicate the SVM performs better than KNN. Maybe the general assumption in the SVM, the existence of a hyper-plane that separate the data points, is less helpful for vigilance datasets of this study. Thus, the non-parametric approximation of the underlying distribution of the dataset, which is the basis for KNN, might result in better accuracies presented in Table 5. Among the classifiers, GBT

performed the best for all the subjects as shown in Table 5. Thus, it was selected for vigilance detection in all locomotion state in this study. As the purpose of the study was to detect vigilance level during walking compared to the seated state, we used classification accuracy as the matric for evaluation though efficiency in respect of algorithm complexity and time cost is also important. To get an essence of these matrics, we calculated the execution time of the GBT to classify a subject's vigilance level. It took 22.56s to complete the classification of subject 1's dataset.

All the classification accuracies from all the datasets are presented in Table 6. For seated state datasets, the mean classification accuracy across all subjects is 89.22%, with a standard error of 0.79%. For the walking datasets, the mean classification accuracy was 85.98% with 1.05% standard error, whereas it improved to 87.20% with 1.08% standard error while motion artifacts removal was applied on the fNIRS signals.

The highest classification accuracy for the seated dataset resulted in subject 2 which was 92.44% and, for the walking dataset, it resulted in subject 7 which was 92.43% and 92.01% for the case of with and without artifacts removal respectively on walking state fNIRS signals.

Regarding the statistical analysis, a two-sample t-test was used to test the statistical significance of the differences in the mean classification accuracies for each walking state to the seated state. The t-test hypotheses testing decisions indicated that the mean classification accuracy of the walking state was statistically different from the mean classification accuracy of the seated state, while no artifacts removal was applied to the walking state dataset. This phenomenon is presented by the significance-link with the star in Figure 15. On the other hand, the classification accuracy of the walking state dataset

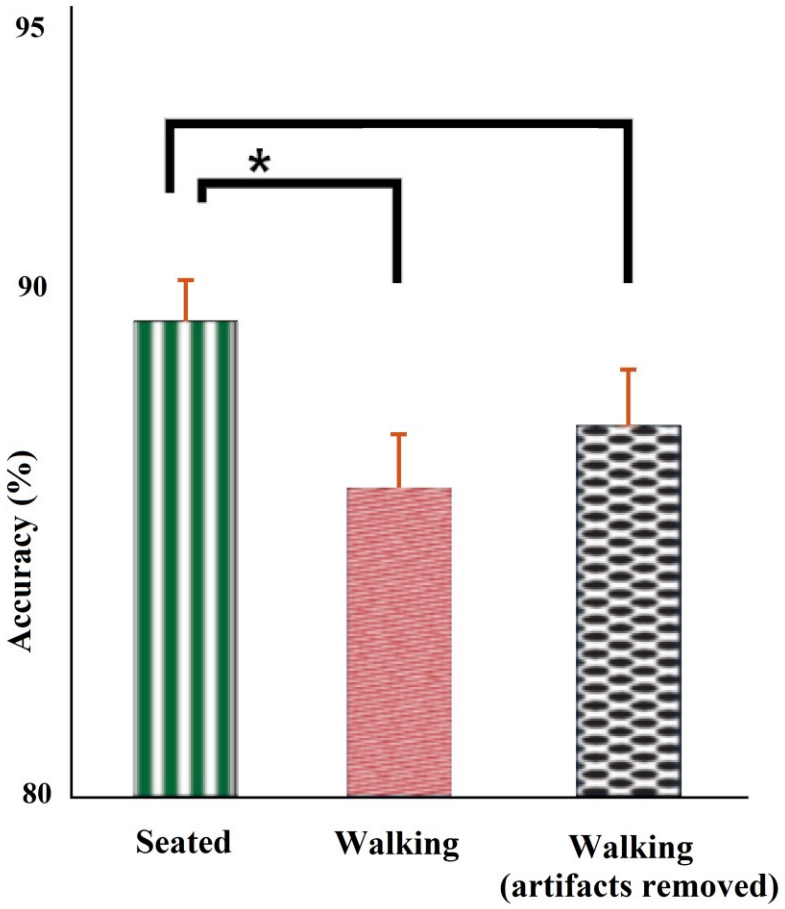

Figure 15. Mean accuracy of classifications for seated state, walking state and walking state with artifact removal. The Standard errors of the mean classification accuracies are presented by the errorbars. The classification accuracies mean whose differences are statistically significant, are presented by the significance-link with the star.

while the artifacts were removed is statistically comparable to the seated state cognitive workload classification accuracy although the difference in the mean accuracy is low.

In the last few decades, fNIRS has been used to detect the neural activity of the human brain in various situations such as cognitive tasks [86], limb movement [145], functional motor activity [146], [147] and so on [80], [88], [148]. In the advent of the use of fNIRS for brain imaging, the researchers focused on the comparison of this modality with other modality of brain imaging [149], [150]. In these comparisons, the metric of interest was the signal waveform correspondence towards the cognitive or non-cognitive activity. To get the hypothesized outcomes in these studies, the factors distorting the waveforms in

those studies are human resting-state physiological variables, such as heart rate, breathing rates and Mayer wave, which are mentioned earlier. A lot of researches focusing on the physiological interferences on fNIRS helped in making it widely accepted to use very low-frequency bandpass to mitigate this issue [151], [152].

This generic methodology of fNIRS signal interference removal, whose basis is the non-movement state of the subject, has been relied on even when the studies involved human walking-related fNIRS studies. For instance, brain activation detection during walking by Mirelman et al. [132], attention-demanding locomotion study by Holtzer et al. [137], [138], hemodynamic of gait kinematics and PFC activation by Lin et al. [129], and so on. However, in this study, we have seen that the fNIRS signals get heavily distorted by the movement artifacts, which is apparent from Figure 14. Figure 14 depicts that motion artifacts distort the signal at 1-back signals by 3 to 7 μmol approximately. In contrast, the 2-back signals were distorted by only 1 to 3 μmol. The uncertainty due to this distortion of the signal resulted in the outcome of this study, where we have seen that the classification accuracy of the walking state vigilance when this distortion is not corrected, is lower than the classification accuracy of the vigilance for the seated state depicted in Table 6.

As the technological advancement enhancing the use of fNIRS from the human sedentary state to the mobile state, the motion-related challenge in fNIRS signal processing needs special attention. The main challenge imposed by motion in the fNIRS signal is the unknow stationarity of the impact of the motions on the fNIRS signals [64]. The low-frequency domain-specific usable information-carrying property of this modality imposes additional difficulty in separating the accurate hemodynamic signal from the

detected fNIRS signals when the motion impacts are present in the signal. In this regard, it is known that the motion artifacts impact the Optode of the fNIRS system and alter the interfacing of the Optode to the human skin [47]. In our previous study, we showed that this alteration of the interfacing of the Optode to the skin can best be captured using sensors specific to motion artifacts, and a more accurate motion signal resulted in the better model to estimate the motion artifacts in the fNIRS signal more accurately.

As the leading player corrupting the fNIRS signal during walking is the motion artifacts, it was necessary to investigate, for better usability of fNIRS modality, how this factor affecting the classification accuracy of the vigilance in walking state compared to a ground truth state where this player is not present which is the seated state. The key challenge of this comparison is that minimization of the variability arises from experimental design such as tasks, responses, task implementation, fNIRS system constrain and so on. To minimize variability, arise from these factors, we strictly maintain the same experimental procedure in both the seated and walking state and the only difference in these two states was walking. In this regard, a question might come why we didn't choose the standing instead of seated as the ground truth state. Some previous studies showed that maintaining balance during standing also required cognitive resources and this effort to maintain balance is also part of walking[153], [154]. Moreover, in this experiment, the signal processing pipeline and the vigilance classification framework has been followed precisely the same in both seated and walking state. The vigilance classification accuracy of the seated and walking state in this study reveals that the classification accuracies of these states are very close in number,

though the walking state vigilance classification is lower than the seated state classification accuracy when no artifacts removal is applied on the walking state signals.

Although the difference in these two mean classification accuracies are small, the statistical test analysis depicts that the distributions of the classification accuracies are significantly different, which is also denoted by the star in Figure 15. Thus, the motion artifacts in walking state fNIRS need special treatment to get the appropriate insight from the fNIRS signals. On the other hand, the mean classification accuracy of the walking state fNIRS signal improved by minimal amount when motion artifacts removal applied on the signal; however, it dramatically improves the distribution of the classification accuracies. Thus, the mean classification accuracies of the walking state vigilance get statistically comparable to the seated state when the motion artifacts were removed from the fNIRS signal [155].

5.5 Conclusions

Vigilance is one of the most vital cognitive functions carried out by the human brain. Among all the state-of-the-art modalities of human brain sensing, fNIRS is one of the most suitable modalities for vigilance detection in ubiquitous human states such as seated as well as walking. However, the motion artifacts were limiting the use of fNIRS modality in the detection of human vigilance only to the sedentary state. In this regard, there are some attempts in taking fNIRS modality to detect human cognitive state during walking; however, the impact of motion artifacts on the fNIRS signal was not treated properly. Whereas, in this study, the quantitative and qualitative result reveals that motion artifacts greatly distort the fNIRS signal. This distortion of the fNIRS signal in the walking state significantly lowers the vigilance detection accuracy compared to the

vigilance detection from seated state fNIRS signals as ground-choose. The methodology presented in this article for the motion sensor signal fusion with the fNIRS optical signal to estimate more accurate hemodynamic signals can result in better detection of vigilance during gait.

REFERENCES

[1] B. S. Oken, M. C. Salinsky, and S. M. Elsas, 'Vigilance, alertness, or sustained attention: physiological basis and measurement', *Clin. Neurophysiol.*, vol. 117, no. 9, 2006.

[2] B. Rypma and M. D. ' Esposito, 'The roles of prefrontal brain regions in components of working memory: Effects of memory load and individual differences', *Proc. Natl. Acad. Sci.*, vol. 96, pp. 6558–6563, 1999.

[3] C. Iadecola and M. Nedergaard, 'Glial regulation of the cerebral microvasculature', *Nat. Neurosci.*, vol. 10, 2007.

[4] S. G. Hart and L. E. Staveland, 'Development of NASA-TLX (Task Load Index): Results of empirical and theoretical research.', *Adv. Psychol.*, vol. 52, pp. 139–183, 1988.

[5] J. D. Cohen *et al.*, 'Temporal dynamics of Brain activation during a working memory task', *Nature*, vol. 386, pp. 604–608, 1997.

[6] H. R. Heekeren, S. Marrett, P. A. Bandettini, and L. G. Ungerleider, 'A general mechanism for perceptual decision-making in the human brain', *Nature*, vol. 431, no. 7010, pp. 859–862, Oct. 2004.

[7] F. Putze *et al.*, 'Hybrid fNIRS-EEG based classification of auditory and visual perception processes', *Front. Neurosci.*, vol. 8, no. OCT, pp. 1–13, 2014.

[8] E. B. J. Coffey, A.-M. Brouwer, and J. B. F. Van Erp, 'Measuring workload using a combination of electroencephalography and near infrared spectroscopy', *Proc. Hum. Factors Ergon. Soc. Annu. Meet.*, vol. 56, no. 1, pp. 1822–1826, 2012.

[9] N. K. Logothetis, J. Pauls, M. Augath, T. Trinath, and A. Oeltermann, 'Neurophysiological investigation of the basis of the fMRI signal', *Nature*, vol. 412, 2001.

[10] E. B. Ringelstein, B. Kahlscheuer, E. Niggemeyer, and S. M. Otis, 'Transcranial Doppler sonography: anatomical landmarks and normal velocity values', *Ultrasound Med. Biol.*, vol. 16, no. 8, pp. 745–761, 1990.

[11] M. Ferrari and V. Quaresima, 'A brief review on the history of human functional near-infrared spectroscopy (fNIRS) development and fields of application', *Neuroimage*, vol. 63, no. 2, pp. 921–935, 2012.

[12] S. Ogawa, T. M. Lee, A. R. Kay, and D. W. Tank, 'Brain magnetic resonance imaging with contrast dependent on blood oxygenation', *Proc. Natl. Acad. Sci.*, vol. 87, pp. 9868–9872, 1990.

[13] S. B. Erdoğan, M. A. Yücel, and A. Akın, 'Analysis of task-evoked systemic interference in fNIRS measurements: Insights from fMRI', *Neuroimage*, vol. 87, pp. 490–504, 2014.

[14] F. A. Fishburn, M. E. Norr, A. V. Medvedev, and C. J. Vaidya, 'Sensitivity of fNIRS to cognitive state and load', *Front. Hum. Neurosci.*, vol. 8, no. February, pp. 1–11, 2014.

[15] S. Wijeakumar, T. J. Huppert, V. A. Magnotta, A. T. Buss, and J. P. Spencer, 'Validating an image-based fNIRS approach with fMRI and a working memory task', *Neuroimage*, vol. 147, pp. 204–218, Feb. 2017.

[16] X. Cui, S. Bray, D. M. Bryant, G. H. Glover, and A. L. Reiss, 'A quantitative comparison of NIRS and fMRI across multiple cognitive tasks', *Neuroimage*, vol. 54, no. 4, pp. 2808–2821, 2011.

[17] J. W. Barker, A. Aarabi, and T. J. Huppert, 'Autoregressive model based algorithm for correcting motion and serially correlated errors in fNIRS', *Biomed. Opt. Express*, vol. 4, no. 8, p. 1366, 2013.

[18] L. Gagnon *et al.*, 'Quantification of the cortical contribution to the NIRS signal over the motor cortex using concurrent NIRS-fMRI measurements', *Neuroimage*, vol. 59, pp. 3933–3940, 2012.

[19] C. Berka *et al.*, 'EEG Correlates of Task Engagement and Mental Workload in Vigilance, Learning, and Memory Tasks', *Aviat. Space. Environ. Med.*, vol. 78, no. 5, 2007.

[20] A. Gevins, M. E. Smith, L. McEvoy, and D. Yu, 'High-resolution EEG mapping of cortical activation related to working memory: effects of task difficulty, type of processing, and practice.', *Cereb. cortex (New York, NY 1991)*, vol. 7, no. 4, pp. 374–385, 1997.

[21] A. Gevins *et al.*, 'Monitoring working memory load during computer-based tasks with EEG pattern recognition methods', *Hum. Factors*, vol. 40, no. 1, pp. 79–91, 1998.

[22] J. S. Warm, R. Parasuraman, and G. Matthews, 'Vigilance Requires Hard Mental Work and Is Stressful', *Hum. Factors J. Hum. Factors Ergon. Soc.*, vol. 50, no. 3, pp. 433–441, Jun. 2008.

[23] J. M. Vettel *et al.*, '2018 Human Variability Workshop: Insights to Drive Scientific Innovations for Human State Detection and Prediction'.

[24] L. Bruyn Martin and C. Karthaus, 'Cognitive Task Analysis of Improvised Explosive Device Detection and Assessment in Canadian Forces Convoy', 2009.

[25] G. Wulf and W. Prinz, ‘Directing attention to movement effects enhances learning: A review’, *Psychon. Bull. Rev.*, vol. 8, no. 4, pp. 648–660, 2001.

[26] R. Sottilare and A. Sinatra, ‘Adaptive Tutoring for Self-Regulated Learning: A Tutorial on Tutoring Systems’, no. December, 2014.

[27] J. J. Laviola, B. M. Williamson, C. Brooks, S. Veazanchin, R. Sottilare, and P. Garrity, ‘Using Augmented Reality to Tutor Military Tasks in the Wild’, in *Proceedings of the Interservice/Industry Training Simulation & Education Conference*, 2015.

[28] H. Ayaz, P. A. Shewokis, S. Bunce, K. Izzetoglu, B. Willems, and B. Onaral, ‘Optical brain monitoring for operator training and mental workload assessment’, *Neuroimage*, vol. 59, no. 1, pp. 36–47, 2012.

[29] T. Kojima, H. Tsunashima, and T. Y. Shiozawa, ‘Measurement of train driver’s brain activity by functional near-infrared spectroscopy (fNIRS)’, *Opt. Quantum Electron.*, vol. 37, 2005.

[30] H. Tsunashima and K. Yanagisawa, ‘Measurement of Brain Function of Car Driver Using Functional Near-Infrared Spectroscopy (fNIRS)’, *Comput. Intell. Neurosci.*, vol. 2009, pp. 1–12, 2009.

[31] R. Parasuraman, ‘Neuroergonomics: Research and practice’, *Theor. issues Ergon. Sci.*, vol. 4, no. 1–2, pp. 5–20, 2003.

[32] A. Villringer and B. Chance, ‘Non-invasive optical spectroscopy and imaging of human brain function.’, *Trends Neurosci*, vol. 20, no. 10, pp. 435–442, 1997.

[33] F. Scholkmann *et al.*, ‘A review on continuous wave functional near-infrared spectroscopy and imaging instrumentation and methodology’, *Neuroimage*, vol. 85, pp. 6–27, 2014.

[34] T. W. L. Scheeren, P. Schober, and L. A. Schwarte, ‘Monitoring tissue oxygenation by near infrared spectroscopy (NIRS): background and current applications’, *J. Clin. Monit. Comput.*, vol. 26, no. 4, pp. 279–287, 2012.

[35] F. Jobsis, ‘Noninvasive, infrared monitoring of cerebral and myocardial oxygen sufficiency and circulatory parameters’, *Science (80-.).*, vol. 198, no. 4323, pp. 1264–1267, 1977.

[36] R. M. Oemrawsingh *et al.*, ‘Near-Infrared Spectroscopy Predicts Cardiovascular Outcome in Patients With Coronary Artery Disease’, *J. Am. Coll. Cardiol.*, vol. 64, no. 23, pp. 2510–2518, 2014.

[37] D. E. Skarda, K. E. Mulier, D. E. Myers, J. H. Taylor, and G. J. Beilman, ‘Dynamic near-infrared spectroscopy measurements in patients with severe sepsis’, *Shock*, vol. 27, no. 4, pp. 348–353, 2007.

[38] J. León-Carrion *et al.*, 'The hemodynamics of cognitive control: The level of concentration of oxygenated hemoglobin in the superior prefrontal cortex varies as a function of performance in a modified Stroop task', *Behav. Brain Res.*, vol. 193, no. 2, pp. 248–256, 2008.

[39] A. Villringer, J. Planck, C. Hock, L. Schleinkofer, and U. Dirnagl, 'Near infrared spectroscopy (NIRS): A new tool to study hemodynamic changes during activation of brain function in human adults', *Neurosci. Lett.*, vol. 154, no. 1–2, pp. 101–104, May 1993.

[40] L. Holper, T. Muehlemann, F. Scholkmann, K. Eng, D. Kiper, and M. Wolf, 'Testing the potential of a virtual reality neurorehabilitation system during performance of observation, imagery and imitation of motor actions recorded by wireless functional near-infrared spectroscopy (fNIRS)', *J. Neuroeng. Rehabil.*, vol. 7, no. 1, pp. 1–13, 2010.

[41] N. Akter, M. Karabiyik, and N. Pala, 'Highly Tunable, Flexible and Stretchable Frequency Selective Surface-Based THz Bandpass Filter', in *2019 IEEE Photonics Conference (IPC)*, pp. 1–2.

[42] M. Karabiyik, N. Akter, and N. Pala, 'On-Chip Spectrometer using Cascaded Echelle Gratings and Arrayed Waveguide Gratings', in *2019 IEEE Research and Applications of Photonics in Defense Conference (RAPID)*, 2019, pp. 1–4.

[43] M. Karabiyik, N. Akter, N. Pala, and B. I. Akca, 'Raman Signal Amplification in Photonic Crystal Microring Resonators', in *2019 IEEE Photonics Conference (IPC)*, 2019, pp. 1–2.

[44] N. Akter, M. Karabiyik, and N. Pala, 'Hybrid Toroidal Modes in Planar Core-Shell Metamaterial Structures', in *2018 IEEE Photonics Conference (IPC)*, pp. 1–2.

[45] S. M. A. Salehizadeh, 'Motion and Noise Artifact Detection and Vital Signal Reconstruction in ECG/PPG based Wearable Devices', *Dr. Diss.*, 2015.

[46] T. E. J. Noponen, K. Kotilahti, I. Nissilä, T. Kajava, and P. T. Meriläinen, 'Effects of improper source coupling in frequency-domain near-infrared spectroscopy', *Phys. Med. Biol.*, vol. 55, no. 10, pp. 2941–2960, 2010.

[47] M. Schweiger, I. Nissilä, D. A. Boas, and S. R. Arridge, 'Image reconstruction in optical tomography in the presence of coupling errors', *Appl. Opt.*, vol. 46, no. 14, pp. 2743–2756, 2007.

[48] F. Scholkmann, A. J. Metz, and M. Wolf, 'Measuring tissue hemodynamics and oxygenation by continuous-wave functional near-infrared spectroscopy - How robust are the different calculation methods against movement artifacts?', *Physiol. Meas.*, vol. 35, no. 4, pp. 717–734, 2014.

[49] K. T. Sweeney, H. Ayaz, T. E. Ward, M. Izzetoglu, S. F. McLoone, and B. Onaral, 'A methodology for validating artifact removal techniques for physiological signals', *IEEE Trans. Inf. Technol. Biomed.*, vol. 16, no. 5, pp. 918–926, 2012.

[50] F. Scholkmann, S. Spichtig, T. Muehlemann, and M. Wolf, 'How to detect and reduce movement artifacts in near-infrared imaging using moving standard deviation and spline interpolation', *Physiol. Meas.*, vol. 31, no. 5, pp. 649–662, 2010.

[51] B. Molavi and G. A. Dumont, 'Wavelet-based motion artifact removal for functional near-infrared spectroscopy', *Physiol. Meas.*, vol. 33, no. 2, pp. 259–270, 2012.

[52] F. C. Robertson, T. S. Douglas, and E. M. Meintjes, 'Motion Artifact Removal for Functional Near Infrared Spectroscopy: A Comparison of Methods', *IEEE Trans. Biomed. Eng.*, vol. 57, no. 6, pp. 1377–1387, 2010.

[53] X. Cui, S. Bray, and A. L. Reiss, 'Functional near infrared spectroscopy (NIRS) signal improvement based on negative correlation between oxygenated and deoxygenated hemoglobin dynamics', *Neuroimage*, vol. 49, no. 4, pp. 3039–3046, 2010.

[54] M. Izzetoglu, P. Chitrapu, S. Bunce, and B. Onaral, 'Motion artifact cancellation in NIR spectroscopy using discrete Kalman filtering.', *Biomed. Eng. Online*, vol. 9, p. 16, 2010.

[55] and B. O. Meltem Izzetoglu*, Ajit Devaraj, Scott Bunce, 'Motion Artifact Cancellation in NIR Spectroscopy Using Wiener Filtering', *IEEE Trans. Biomed. Eng.*, vol. 52, no. 5, pp. 2–5, 2005.

[56] A. Hossen, M. Muthuraman, J. Raethjen, G. Deuschl, and U. Heute, 'Discrimination of parkinsonian tremor from essential tremor by implementation of a wavelet-based soft-decision technique on emg and accelerometer signals', *Biomed. Signal Process. Control*, vol. 5, no. 3, pp. 181–188, 2010.

[57] S. Lawoyin, D.-Y. Fei, and O. Bai, 'Accelerometer-based steering-wheel movement monitoring for drowsy-driving detection', *Proc. Inst. Mech. Eng. Part D J. Automob. Eng.*, vol. 229, no. 2, pp. 163–173, Feb. 2015.

[58] S. Lawoyin, D.-Y. Fei, O. Bai, and X. Liu, 'Evaluating the efficacy of an accelerometer–based method for drowsy driving detection', *Int. J. Veh. Saf.*, vol. 8, no. x, p. pp 165-179, 2015.

[59] O. Bai, R. Atri, J. S. Marquez, and D.-Y. Fei, 'Characterization of lower limb activity during gait using wearable, multi-channel surface EMG and IMU sensors', *2017 Int. Electr. Eng. Congr.*, no. March, pp. 1–4, 2017.

[60] S. Lawoyin, X. Liu, D. Y. Fei, and O. Bai, 'Detection methods for a low-cost accelerometer-based approach for driver drowsiness detection', *Conf. Proc. - IEEE Int. Conf. Syst. Man Cybern.*, vol. 2014-Janua, no. January, pp. 1636–1641, 2014.

[61] S. A. Lawoyin, D.-Y. Fei, and O. Bai, 'A Novel Application of Inertial Measurement Units (IMUs) as Vehicular Technologies for Drowsy Driving Detection via Steering Wheel Movement', *Open J. Saf. Sci. Technol.*, vol. 04, no. 04, pp. 166–177, 2014.

[62] J. Virtanen, T. Noponen, K. Kotilahti, J. Virtanen, and R. J. Ilmoniemi, 'Accelerometer-based method for correcting signal baseline changes caused by motion artifacts in medical near-infrared spectroscopy', *J. Biomed. Opt.*, vol. 16, no. 8, p. 087005, 2011.

[63] S. H. Kim, D. W. Ryoo, and C. Bae, 'Adaptive noise cancellation using accelerometers for the PPG signal from forehead.', *Conf. Proc. IEEE Eng. Med. Biol. Soc.*, vol. 2007, pp. 2564–2567, 2007.

[64] M. Izzetoglu, A. Devaraj, S. Bunce, and B. Onaral, 'Motion artifact cancellation in NIR spectroscopy using Wiener filtering', *IEEE Trans. Biomed. Eng.*, vol. 52, no. 5, pp. 934–938, May 2005.

[65] C. K. Kim, S. Lee, D. Koh, and B. M. Kim, 'Development of wireless NIRS system with dynamic removal of motion artifacts', *Biomed. Eng. Lett.*, vol. 1, no. 4, pp. 254–259, 2011.

[66] R. J. Cooper *et al.*, 'A systematic comparison of motion artifact correction techniques for functional near-infrared spectroscopy', *Front. Neurosci.*, vol. 6, no. OCT, pp. 1–10, 2012.

[67] B. Widrow *et al.*, 'Adaptive Noise Cancelling: Principles and Applications', *Proc. IEEE*, vol. 63, no. 12, pp. 1692–1716, 1975.

[68] M. Cope, 'The development of a near infrared spectroscopy system and its application for non invasive monitory of cerebral blood and tissue oxygenation in the newborn infants', *Diss. Univ. London*, p. 342, 1991.

[69] S. Wray, M. Cope, D. T. Delpy, J. S. Wyatt, and E. O. R. Reynolds, 'Characterization of the near infrared absorption spectra of cytochrome aa3 and haemoglobin for the non-invasive monitoring of cerebral oxygenation', *Biochim. Biophys. Acta - Bioenerg.*, vol. 933, no. 1, pp. 184–192, Mar. 1988.

[70] Y. Wang *et al.*, 'A multifunctional wireless body area sensors network with real time embedded data analysis', *2016 IEEE Biomed. Circuits Syst. Conf. BioCAS 2016*, pp. 508–511, 2016.

[71] K. T. Sweeney, S. F. McLoone, and T. E. Ward, 'The use of ensemble empirical mode decomposition with canonical correlation analysis as a novel artifact removal technique', *IEEE Trans. Biomed. Eng.*, vol. 60, no. 1, pp. 97–105, 2013.

[72] B. E. Boser and R. T. Howe, 'Surface micromachined accelerometers', *IEEE J. Solid-State Circuits*, vol. 31, no. 3, pp. 366–375, 1996.

[73] S. Brigadoi *et al.*, 'Motion artifacts in functional near-infrared spectroscopy: A comparison of motion correction techniques applied to real cognitive data', *Neuroimage*, vol. 85, pp. 181–191, 2014.

[74] K. E. Y. Ronald E. Walplte, Raymond H. Myers, Sharon L. Myers, *Probability and statistics for Engineers & Scientists*, 9th ed. Prentice Hall, 2011.

[75] R. A. Khan, N. Naseer, N. Khalid Qureshi, F. M. Noori, H. Nazeer, and M. U. Khan, 'fNIRS-based Neurorobotic Interface for gait rehabilitation', *J. Neuroeng. Rehabil.*, 2018.

[76] M. Rea *et al.*, 'Lower Limb Movement Preparation in Chronic Stroke', *Neurorehabil. Neural Repair*, vol. 28, no. 6, pp. 564–575, 2014.

[77] K. S. Hong, N. Naseer, and Y. H. Kim, 'Classification of prefrontal and motor cortex signals for three-class fNIRS-BCI', *Neurosci. Lett.*, vol. 587, pp. 87–92, 2015.

[78] W. Jia, D. Huang, X. Luo, H. Pu, X. Chen, and O. Bai, 'Electroencephalography(EEG)-based instinctive brain-control of a quadruped locomotion robot', *Proc. Annu. Int. Conf. IEEE Eng. Med. Biol. Soc. EMBS*, pp. 1777–1781, 2012.

[79] P. Pinti *et al.*, 'A Review on the Use of Wearable Functional Near-Infrared Spectroscopy in Naturalistic Environments', *Jpn. Psychol. Res.*, vol. 60, no. 4, pp. 347–373, 2018.

[80] N. Naseer and K.-S. Hong, 'fNIRS-based brain-computer interfaces: a review', *Front. Hum. Neurosci.*, vol. 9, no. January, pp. 1–15, 2015.

[81] M. R. Siddiquee, J. S. Marquez, R. Atri, R. Ramon, R. Perry Mayrand, and O. Bai, 'Movement artefact removal from NIRS signal using multi-channel IMU data', *Biomed. Eng. Online*, vol. 17, no. 1, p. 120, 2018.

[82] W. Elmenreich, 'An introduction to sensor fusion', *Vienna Univ. Technol.*, vol. 502, no. February, pp. 1–28, 2002.

[83] A. H. Jalal, F. Alam, S. Roychoudhury, Y. Umasankar, N. Pala, and S. Bhansali, 'Prospects and challenges of volatile organic compound sensors in human healthcare', *ACS sensors*, vol. 3, no. 7, pp. 1246–1263, 2018.

[84] F. Alam *et al.*, 'Lactate biosensing: The emerging point-of-care and personal health monitoring', *Biosens. Bioelectron.*, vol. 117, pp. 818–829, 2018.

[85] G. Li, S. P. Baker, J. G. Grabowski, and G. W. Rebok, 'Factors Associated with Pilot Error in Aviation Crashes', *Aviat. Space. Environ. Med.*, vol. 72, no. 1, pp. 52–58, 2001.

[86] C. Herff *et al.*, 'Mental workload during n-back task—quantified in the prefrontal cortex using fNIRS', *Front. Hum. Neurosci.*, 2014.

[87] H. Aghajani, M. Garbey, and A. Omurtag, 'Measuring Mental Workload with EEG+fNIRS', *Front. Hum. Neurosci.*, vol. 11, no. July, pp. 1–20, 2017.

[88] K. Yamamoto, H. Takahashi, T. Kato, N. Oka, and K. Yoshino, 'Functional brain imaging using near-infrared spectroscopy during actual driving on an expressway', *Front. Hum. Neurosci.*, vol. 7, no. December, pp. 1–16, 2013.

[89] M. Causse, Z. Chua, V. Peysakhovich, N. Del Campo, and N. Matton, 'Mental workload and neural efficiency quantified in the prefrontal cortex using fNIRS', *Sci. Rep.*, vol. 7, no. 1, 2017.

[90] M. Paczynski *et al.*, 'Into the Wild: Neuroergonomic Differentiation of Hand-Held and Augmented Reality Wearable Displays during Outdoor Navigation with Functional Near Infrared Spectroscopy', *Front. Hum. Neurosci.*, vol. 10, no. May, pp. 1–15, 2016.

[91] P. Pinti *et al.*, 'Using Fiberless, Wearable fNIRS to Monitor Brain Activity in Real-world Cognitive Tasks', *J. Vis. Exp*, no. 106, p. 53336, 2015.

[92] H. Atsumori, 'Noninvasive imaging of prefrontal activation during attention-demanding tasks performed while walking using a wearable optical topography system', *J. Biomed. Opt.*, vol. 15, no. 4, p. 046002, 2010.

[93] A. Baddeley, 'Working memory: looking back and looking forward.', *Nat. Rev. Neurosci.*, vol. 4, no. 10, 2003.

[94] A. M. Owen, K. M. McMillan, A. R. Laird, and E. Bullmore, 'N-back working memory paradigm: A meta-analysis of normative functional neuroimaging studies', *Hum. Brain Mapp.*, vol. 25, no. 1, pp. 46–59, 2005.

[95] K. Mandrick, G. Derosiere, G. Dray, D. Coulon, J.-P. Micallef, and S. Perrey, 'Prefrontal cortex activity during motor tasks with additional mental load requiring attentional demand: A near-infrared spectroscopy study', *Neurosci. Res.*, vol. 76, pp. 156–162, 2013.

[96] N. R. de Joux, K. M. Wilson, P. N. Russell, K. M. Finkbeiner, and W. S. Helton, 'A functional near-infrared spectroscopy study of the effects of configural properties on sustained attention', *Neuropsychologia*, vol. 94, pp. 106–117, Jan. 2017.

[97] W. K. Kirchner, 'Age differences in short-term retention of rapidly changing information', *J. Exp. Psychol.*, vol. 55, no. 4, 1958.

[98] P. Hoskinson and J. Toomim, 'Brain workshop – a dual N-Back game'. 2009.

[99] Y. Tomita, F. B. Vialatte, G. Dreyfus, Y. Mitsukura, H. Bakardjian, and A. Cichocki, 'Bimodal BCI using simultaneously NIRS and EEG', *IEEE Trans. Biomed. Eng.*, vol. 61, no. 4, pp. 1274–1284, 2014.

[100] C. E. Elwell, R. Springett, E. Hillman, and D. T. Delpy, 'Oscillations in cerebral haemodynamics', in *Oxygen transport to tissue XXI*, Springer, 1999, pp. 57–65.

[101] M. A. Rahman, M. A. Rashid, and M. Ahmad, 'Selecting the optimal conditions of Savitzky–Golay filter for fNIRS signal', *Biocybern. Biomed. Eng.*, vol. 39, no. 3, pp. 624–637, 2019.

[102] S. D. Power, A. Kushki, and T. Chau, 'Intersession Consistency of Single-Trial Classification of the Prefrontal Response to Mental Arithmetic and the No-Control State by NIRS', *PLoS One*, vol. 7, no. 7, 2012.

[103] A. Faress and T. Chau, 'Towards a multimodal brain-computer interface: Combining fNIRS and fTCD measurements to enable higher classification accuracy', *Neuroimage*, vol. 77, pp. 186–194, 2013.

[104] S. Moghimi, A. Kushki, S. Power, A. M. Guerguerian, and T. Chau, 'Automatic detection of a prefrontal cortical response to emotionally rated music using multi-channel near-infrared spectroscopy', *J. Neural Eng.*, vol. 9, 2012.

[105] L. Holper and M. Wolf, 'Single-trial classification of motor imagery differing in task complexity: a functional near-infrared spectroscopy study', *J. Neuroeng. Rehabil.*, 2011.

[106] M. J. Khan and K.-S. Hong, 'Passive BCI based on drowsiness detection: an fNIRS study', *Biomed. Opt. Express*, vol. 6, no. 10, pp. 4063–4078, 2015.

[107] X. Cui, S. Bray, and A. L. Reiss, 'Speeded Near Infrared Spectroscopy (NIRS) Response Detection', *PLoS One*, vol. 5, no. 11, p. 15474, 2010.

[108] R. Sitaram *et al.*, 'Temporal classification of multichannel near-infrared spectroscopy signals of motor imagery for developing a brain-computer interface', 2006.

[109] S. Shrestha, S. A. Morshed, N. Pradhananga, and X. LV, ‘Leveraging Accident Investigation Reports As Leading Indicators Of Construction Safety Using Text Classification’, in *ASCE Construction Research Congress (CRC) 2020*, 2020.

[110] L. Jahan, G. Chauhan, and M. Finlayson, ‘A new approach to animacy detection’, in *Proceedings of the 27th International Conference on Computational Linguistics*, 2018, pp. 1–12.

[111] S. M. S. Hasan, M. R. Siddiquee, and O. Bai, ‘Supervised Classification of EEG Signals with Score Threshold Regulation for Pseudo-online Asynchronous Detection of Gait Intention’, in *2019 18th IEEE International Conference On Machine Learning And Applications (ICMLA)*, 2019, pp. 1476–1479.

[112] R. Atri *et al.*, ‘Smart data-driven optimization of powered prosthetic ankles using surface electromyography’, *Sensors*, vol. 18, no. 8, pp. 1–19, 2018.

[113] N. Thanh Hai, N. Q. Cuong, T. Q. Dang Khoa, and V. Van Toi, ‘Temporal hemodynamic classification of two hands tapping using functional near—infrared spectroscopy’, *Front. Hum. Neurosci.*, vol. 7, no. September, pp. 1–12, 2013.

[114] B. Abibullaev, J. An, and J.-I. Moon, ‘Neural Network Classification of Brain Hemodynamic Responses from Four Mental Tasks’, *Int. J. Optomechatronics*, vol. 5, no. 4, pp. 340–359, Oct. 2011.

[115] X. Lv, S. A. Morshed, and L. Zhang, ‘Automatic Key-phrase Extraction to Support the Understanding of Infrastructure Disaster Resilience’, in *ISARC. Proceedings of the International Symposium on Automation and Robotics in Construction*, 2019, vol. 36, pp. 1276–1281.

[116] S. Ganzfried and F. Yusuf, ‘Computing human-understandable strategies: deducing fundamental rules of poker strategy’, *Games*, vol. 8, no. 4, p. 49, 2017.

[117] N. Naseer, N. K. Qureshi, F. M. Noori, and K. S. Hong, ‘Analysis of Different Classification Techniques for Two-Class Functional Near-Infrared Spectroscopy-Based Brain-Computer Interface’, *Comput. Intell. Neurosci.*, vol. 2016, 2016.

[118] R. Kohavi and G. H. John, ‘Wrappers for feature subset selection’, *Artifical Intell.*, 1997.

[119] K. Kira and L. A. Rendell, ‘A practical approach to feature selection’, *Mach. Learn. Proc. 1992*, pp. 249–256, 1992.

[120] M. Robnik-ˇ Sikonja and I. Kononenko, ‘Theoretical and Empirical Analysis of ReliefF and RReliefF’, *Mach. Learn.*, vol. 53, pp. 23–69, 2003.

[121] R. Kohavi, ‘A study of cross-validation and bootstrap for accuracy estimation and model selection.’, *In Ijcai*, vol. 14, no. 2, pp. 1137–1145, 1995.

[122] S. Ganzfried and F. Yusuf, ‘Optimal Weighting for Exam Composition’, *Educ. Sci.*, vol. 8, no. 1, p. 36, 2018.

[123] P. Liu *et al.*, ‘Towards Adaptive Replication for Hot/Cold Blocks in HDFS using MemCached’, in *2019 2nd International Conference on Data Intelligence and Security (ICDIS)*, 2019, pp. 188–194.

[124] R. L. Buckner, J. R. Andrews-Hanna, and D. L. Schacter, ‘The brain’s default network: anatomy, function, and relevance to disease’, *Ann. N. Y. Acad. Sci.*, vol. 1124, no. 1, pp. 1–38, 2008.

[125] D. A. Gusnard and M. E. Raichle, ‘Searching for a baseline: functional imaging and the resting human brain’, *Nat. Rev. Neurosci.*, vol. 2, no. 10, p. 685, 2001.

[126] R. Vitorio, S. Stuart, L. Rochester, L. Alcock, and A. Pantall, ‘fNIRS response during walking — Artefact or cortical activity? A systematic review’, *Neurosci. Biobehav. Rev.*, vol. 83, pp. 160–172, Dec. 2017.

[127] S. Brigadoi, A. Ganglani, H. Zhao, and R. J. Cooper, ‘Integrating motion sensing and wearable, modular high-density diffuse optical tomography: preliminary results’, in *European Conference on Biomedical Optics*, 2019, vol. 1107405, no. July 2019, p. 4.

[128] M. R. Siddiquee *et al.*, ‘Sensor Fusion in Human Cyber Sensor System for Motion Artifact Removal from NIRS Signal’, *Int. Conf. Hum. Syst. Interact. HSI*, vol. 2019-June, pp. 192–196, 2019.

[129] M. B. Lin and K. Lin, ‘Walking while Performing Working Memory Tasks Changes the Prefrontal Cortex Hemodynamic Activations and Gait Kinematics’, *Front. Behav. Neurosci.*, vol. 10, no. May, 2016.

[130] S. Oh, M. Song, and J. Kim, ‘Validating attentive locomotion training using interactive treadmill: an fNIRS study’, *J. Neuroeng. Rehabil.*, 2018.

[131] F. G. Metzger *et al.*, ‘Functional brain imaging of walking while talking – An fNIRS study’, *Neuroscience*, vol. 343, pp. 85–93, Feb. 2017.

[132] A. Mirelman *et al.*, ‘Increased frontal brain activation during walking while dual tasking: an fNIRS study in healthy young adults’, *J. Neuroeng. Rehabil.*, 2014.

[133] D. Meester, E. Al-Yahya, H. Dawes, P. Martin-Fagg, and C. Piñon, ‘Associations between prefrontal cortex activation and H-reflex modulation during dual task gait’, *Front. Hum. Neurosci.*, vol. 8, no. 1 FEB, pp. 1–8, 2014.

[134] T. Harada, I. Miyai, M. Suzuki, and K. Kubota, ‘Gait capacity affects cortical activation patterns related to speed control in the elderly’, *Exp Brain Res*, vol. 193, pp. 445–454, 2009.

[135] M. Mihara, I. Miyai, M. Hatakenaka, K. Kubota, and S. Sakoda, 'Sustained prefrontal activation during ataxic gait: A compensatory mechanism for ataxic stroke?', *Neuroimage*, vol. 37, 2007.

[136] R. Holtzer, J. R. Mahoney, M. Izzetoglu, K. Izzetoglu, B. Onaral, and J. Verghese, 'fNIRS Study of Walking and Walking While Talking in Young and Old Individuals', *J. Gerontol. Med. Sci. Cite J. as J Gerontol A Biol Sci Med Sci*, vol. 66, no. 8, pp. 879–887, 2011.

[137] R. Holtzer, J. Verghese, G. Allali, M. Izzetoglu, C. Wang, and J. R. Mahoney, 'Neurological Gait Abnormalities Moderate the Functional Brain Signature of the Posture First Hypothesis', *Brain Topogr.*, vol. 29, 2016.

[138] R. Holtzer, J. R. Mahoney, M. Izzetoglu, C. Wang, S. England, and J. Verghese, 'Online fronto-cortical control of simple and attention-demanding locomotion in humans', *Neuroimage*, vol. 112, pp. 152–159, May 2015.

[139] E. Koechlin, 'An evolutionary computational theory of prefrontal executive function in decision-making', *Philos. Trans. R. Soc. B Biol. Sci.*, vol. 369, 2014.

[140] S. T. Mueller and B. J. Piper, 'The Psychology Experiment Building Language (PEBL) and PEBL Test Battery', *J. Neurosci. Methods*, vol. 222, pp. 250–259, 2014.

[141] J. S. Márquez, R. Atri, M. R. Siddiquee, C. Leung, and O. Bai, 'A Mobile, Smart Gait Assessment System for Asymmetry Detection Using Machine Learning-Based Classification', *J Biomed Eng Med Devic*, vol. 3, no. 1, p. 135, 2018.

[142] I. Maidan *et al.*, 'The Role of the Frontal Lobe in Complex Walking Among Patients With Parkinson's Disease and Healthy Older Adults: An fNIRS Study', *Neurorehabil. Neural Repair*, vol. 30, no. 10, 2016.

[143] A. Orlenko *et al.*, 'Model selection for metabolomics: predicting diagnosis of coronary artery disease using automated machine learning', *Bioinformatics*, no. November, pp. 1–7, 2019.

[144] F. Pedregosa *et al.*, 'Scikit-learn: Machine learning in Python.', *J. Mach. Learn. Res.*, vol. 12, 2011.

[145] M. Suzuki, I. Miyai, T. Ono, and K. Kubota, 'Activities in the frontal cortex and gait performance are modulated by preparation. An fNIRS study', *Neuroimage*, vol. 39, no. 2, pp. 600–607, 2007.

[146] R. Nishiyori, S. Bisconti, and B. Ulrich, 'Motor Cortex Activity During Functional Motor Skills: An fNIRS Study', *Brain Topogr.*, vol. 29, no. 1, pp. 42–55, 2016.

[147] D. R. Leff *et al.*, 'Assessment of the cerebral cortex during motor task behaviours in adults: A systematic review of functional near infrared spectroscopy (fNIRS) studies', *Neuroimage*, 2011.

[148] E. M. Peck, B. F. Yuksel, A. Ottley, R. J. K. Jacob, and R. Chang, 'Using fNIRS Brain Sensing to Evaluate Information Visualization Interfaces', in *Proceedings of the SIGCHI Conference on Human Factors in Computing Systems*, 2013.

[149] G. Strangman, J. P. Culver, J. H. Thompson, and D. A. Boas, 'A Quantitative Comparison of Simultaneous BOLD fMRI and NIRS Recordings during Functional Brain Activation', *Neuroimage*, vol. 17, no. 2, pp. 719–731, 2002.

[150] X. Cui, S. Bray, D. M. Bryant, G. H. Glover, and A. L. Reiss, 'A quantitative comparison of NIRS and fMRI across multiple cognitive tasks', *Neuroimage*, vol. 54, no. 4, pp. 2808–2821, 2011.

[151] E. Kirlilna, N. Yu, A. Jelzow, H. Wabnitz, A. M. Jacobs, and I. Tachtsidis, 'Identifying and quantifying main components of physiological noise in functional near infrared spectroscopy on the prefrontal cortex', *Front. Hum. Neurosci.*, vol. 7, p. 864, Dec. 2013.

[152] Y. Zhang, D. H. Brooks, M. A. Franceschini, and D. A. Boas, 'Eigenvector-based spatial filtering for reduction of physiological interference in diffuse optical imaging', *J. Biomed. Opt.*, vol. 10, no. 1, p. 011014, 2005.

[153] M. Mihara, I. Miyai, M. Hatakenaka, K. Kubota, and S. Sakoda, 'Role of the prefrontal cortex in human balance control', *Neuroimage*, vol. 43, 2008.

[154] F. Herold, K. Orlowski, S. Börmel, and N. G. Müller, 'Cortical activation during balancing on a balance board', *Hum. Mov. Sci.*, 2017.

[155] M. R. Siddiquee, S. M. S. Hasan, J. S. Marquez, R. N. Ramon, and O. Bai, 'Accurate Vigilance Detection During Gait by Using Movement Artifact Removal', *IEEE Access*, vol. 8, pp. 1–1, 2020.

VITA

MASUDUR R. SIDDIQUEE

2016-2020 PhD. Electrical and Computer Engineering
Florida International University
Miami, Florida, USA

2016-2019 M.Sc. Electrical Engineering
Florida International University
Miami, Florida, USA

2008-2009 M.Sc. Applied Physics, Electronics & Communication Engineering
University of Dhaka
Dhaka, Bangladesh

2004-2007 B.Sc. Applied Physics, Electronics & Communication Engineering
University of Dhaka
Dhaka, Bangladesh

PUBLICATIONS

1. Siddiquee, M.R., Marquez, J.S., Atri, R., Ramon, R., Mayrand, R.P. and Bai, O., 2018. Movement artefact removal from NIRS signal using multi-channel IMU data. Biomedical engineering online, 17(1), pp.1-16.

2. Siddiquee, M.R., Xue, T., Marquez, J.S., Atri, R., Ramon, R., Mayrand, R.P., Leung, C. and Bai, O., 2019, June. Sensor Fusion in Human Cyber Sensor System for Motion Artifact Removal from NIRS Signal. In 2019 12th International Conference on Human System Interaction (HSI) (pp. 192-196). IEEE.

3. Siddiquee, M.R., Atri, R., Marquez, J.S., Shafiul, H., Ramon, R., Mayrand, R.P. and Bai, O., 2019. Sensor Location Optimization of Wireless Wearable fNIRS System for Cognitive Workload Monitoring Using a Data Driven Approach for Improved Wear-ability. Submitted In Biocybernetics and Biomedical Engineering.

4. Siddiquee, Masudur R., SM Shafiul Hasan, J. Sebastian Marquez, Rodrigo Nicolas Ramon, and Ou Bai. "Accurate Vigilance Detection During Gait by Using Movement Artifact Removal." IEEE Access 8 (2020): 51179-51188.

5. Hasan, S.S., Siddiquee, M.R. and Bai, O., 2019, December. Supervised Classification of EEG Signals with Score Threshold Regulation for Pseudo-Online Asynchronous Detection of Gait Intention. In 2019 18th IEEE International Conference On Machine Learning And Applications (ICMLA) (pp. 1476-1479). IEEE.

6. Márquez, J.S., Atri, R., Siddiquee, M.R., Leung, C. and Bai, O., 2018. A Mobile, Smart Gait Assessment System for Asymmetry Detection Using Machine Learning-Based Classification. J Biomed Eng Med Devic, 3(135), p.2.

7. Atri, R., Marquez, J.S., Leung, C., Siddiquee, M.R., Murphy, D.P., Gorgey, A.S., Lovegreen, W.T., Fei, D.Y. and Bai, O., 2018. Smart data-driven optimization of powered prosthetic ankles using surface electromyography. Sensors, 18(8), p.2705.